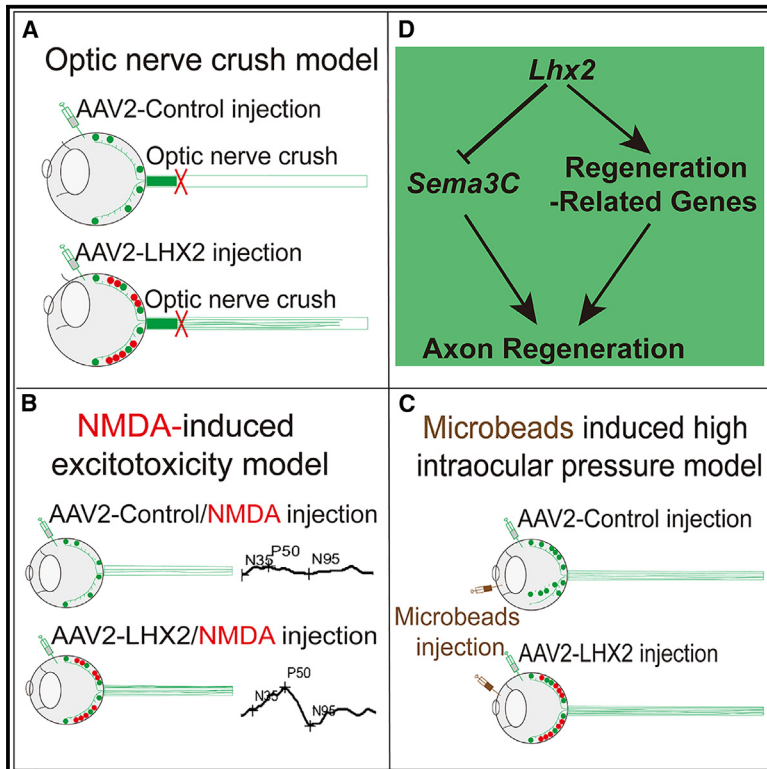


Lhx2 promotes axon regeneration of adult retinal ganglion cells and rescues neurodegeneration in mouse models of glaucoma

Graphical abstract



Authors

Chang-Ping Li, Shen Wu, Yong-Quan Sun, ..., Zhao-Qian Teng, Ningli Wang, Chang-Mei Liu

Correspondence

tengzq@ioz.ac.cn (Z.-Q.T.), wningli@vip.163.com (N.W.), liuchm@ioz.ac.cn (C.-M.L.)

In brief

Li et al. show that overexpression of *Lhx2* promotes RGC survival and axon regeneration after retinal and optic nerve injuries and preserves functional vision. *Sema3C* acts downstream of *Lhx2* in promoting axon regeneration of RGCs.

Highlights

- *Lhx2* promotes axon regeneration of RGCs after axonal injury
- *Lhx2* sustains RGC survival in axonal injury and mouse glaucoma models
- *Lhx2* protects visual pathways and preserves functional vision
- *Sema3C* acts downstream of *Lhx2* in promoting axon regeneration



Article

Lhx2 promotes axon regeneration of adult retinal ganglion cells and rescues neurodegeneration in mouse models of glaucoma

Chang-Ping Li,^{1,2,3,4,8} Shen Wu,^{5,6,8} Yong-Quan Sun,^{1,2,3,4} Xue-Qi Peng,^{1,2,3,4} Maolei Gong,^{1,3,4} Hong-Zhen Du,^{1,3,4} Jingxue Zhang,^{5,6} Zhao-Qian Teng,^{1,2,3,4,9,*} Ningli Wang,^{5,6,7,9,*} and Chang-Mei Liu^{1,2,3,4,9,10,*}

¹Key Laboratory of Organ Regeneration and Reconstruction, Institute of Zoology, Chinese Academy of Sciences, Beijing 100101, China

²Savaid Medical School, University of Chinese Academy of Sciences, Beijing 100049, China

³Institute for Stem Cell and Regeneration, Chinese Academy of Sciences, Beijing 100101, China

⁴Beijing Institute for Stem Cell and Regenerative Medicine, Beijing 100101, China

⁵Beijing Institute of Ophthalmology, Beijing Tongren Eye Center, Beijing Tongren Hospital, Capital Medical University, Beijing Ophthalmology & Visual Sciences Key Laboratory, Beijing 100730, China

⁶Beijing Institute of Brain Disorders, Collaborative Innovation Center for Brain Disorders, Capital Medical University, Beijing 100069, China

⁷Henan Academy of Innovations in Medical Science, Zhengzhou, Henan 450052, China

⁸These authors contributed equally

⁹These authors contributed equally

¹⁰Lead contact

*Correspondence: tengzq@ioz.ac.cn (Z.-Q.T.), wningli@vip.163.com (N.W.), liuchm@ioz.ac.cn (C.-M.L.)

<https://doi.org/10.1016/j.xcr.2024.101554>

SUMMARY

The axons of retinal ganglion cells (RGCs) form the optic nerve, transmitting visual information from the eye to the brain. Damage or loss of RGCs and their axons is the leading cause of visual functional defects in traumatic injury and degenerative diseases such as glaucoma. However, there are no effective clinical treatments for nerve damage in these neurodegenerative diseases. Here, we report that LIM homeodomain transcription factor *Lhx2* promotes RGC survival and axon regeneration in multiple animal models mimicking glaucoma disease. Furthermore, following N-methyl-D-aspartate (NMDA)-induced excitotoxicity damage of RGCs, *Lhx2* mitigates the loss of visual signal transduction. Mechanistic analysis revealed that overexpression of *Lhx2* supports axon regeneration by systematically regulating the transcription of regeneration-related genes and inhibiting transcription of Semaphorin 3C (*Sema3C*). Collectively, our studies identify a critical role of *Lhx2* in promoting RGC survival and axon regeneration, providing a promising neural repair strategy for glaucomatous neurodegeneration.

INTRODUCTION

Axon regeneration in the mature mammalian central nervous system (CNS) is extremely limited after damage. Consequently, functional deficits and neurodegeneration persist after spinal cord injury, traumatic brain injury, stroke, glaucoma, or related conditions that involve axonal disconnection.^{1–3} Failure of axon regeneration is mainly due to external inhibition and intrinsic constraints on growth in mature injured neurons.^{4–6} The external inhibitory molecules of CNS regeneration are usually divided into three categories: axon guidance molecules (epinephrin, neurin, and semaphorins),^{7–9} myelin sheath inhibitors (oligodendrocyte myelin glycoprotein [OMgp], myelin associated glycoprotein [MAG], and Nogo),^{10–14} and chondroitin sulfate proteoglycans (lectin, NG2).^{15,16} Very early studies mainly focused on hostile environment improvements by eliminating these inhibitory factors and promoting axon regeneration in the adult CNS.¹⁷ More recent studies demonstrated that reactivation of neuronal regeneration of injured neurons is another promising strategy for promoting CNS functional recovery. Researchers

have discovered that intrinsic deletion of phosphatase and tenin homolog (PTEN) and suppressor of cytokine signaling 3 (SOCS3), which are negative regulators of the mTOR or JAK-STAT pathway, can dramatically promote axon regeneration of retinal ganglion cells (RGCs).^{18–20} Also, re-expression of regeneration-related molecules, such as SRY-related HMG box 11 (SOX11), RNA-binding protein Lin28, and thrombospondin 1, significantly promote optic nerve regeneration.^{21–24} However, these molecules are still unable to enhance functional recovery and delay neurodegeneration in neurodegenerative diseases despite the improvement in optic nerve regeneration. Therefore, other strategies combined with neuronal survival improvement are urgently required for long-term functional restoration.

Transcription factors (TFs), acting as important regulators of axon growth during development,^{25,26} represent an alternative way to promote axon regeneration in adulthood. Previous studies demonstrated that TFs, including paired box 6 (PAX6), visual system homeobox 2, sine oculis-related homeobox 6, LIM homeobox protein 2 (LHX2), members of the Krüppel-like factor (KLF), and SOX family members, play a key role in the



differentiation of retinal progenitor cells (RPCs) into RGCs.^{27–29} Of note, some of these TFs have been reported to promote neuronal survival and axon regeneration after damage. For example, *Sox11* expression promotes axon regeneration of non- α -RGCs but kills α -RGCs.²¹ Deletion of *KLF4* induces axon regeneration of RGCs through JAK-STAT3 signaling.³⁰ Ectopic expression of *Oct4*, *Sox2*, and *Klf4* in adult mouse RGCs restores youthful DNA methylation patterns and transcriptomes, thereby promoting axon regeneration after optic nerve injury and reversing vision loss in the mouse model of glaucoma and aged mice.³¹ Recently, a combination of *in vivo* CRISPR screening and multi-omic analysis has been used to characterize the core transcription programs controlling injury-induced neurodegeneration of RGCs and reveals novel critical TFs for adult neuronal repair after damage,³² which will provide new strategies for axon regeneration.

Lhx2, a LIM homeodomain TF highly expressed in RPCs, plays an essential role throughout retinogenesis.^{33–36} During retina development, neurons and glia of the retina are derived from RPCs.^{27,28} Deletion of *Lhx2* causes a significant reduction of the progenitor population and a corresponding increase in neurogenesis.³⁷ *Lhx2* is required for all phases of Müller formation, including the proliferation of gliocompetent retinal progenitors, the activation of Müller-specific gene expression, and the ultimate differentiation of Müller morphological characteristics.³⁴ Meanwhile, *Lhx2* regulates retinal Müller gliogenesis by directly inhibiting the expression of components of the Notch signaling pathway.³⁴ Furthermore, the function of *Lhx2* to regulate the coordinated differentiation of neurons and Müller glial cells is controlled by *Ldb1* and *Rnf12* in the postnatal retina.³⁸ However, the role of *Lhx2* in axon regeneration and functional recovery after CNS injury remains unclear.

In our study, by using the optic nerve crush (ONC) model, we found that overexpression of *Lhx2* in adult RGCs significantly promoted axon regeneration. In the delayed therapy model, *Lhx2* promoted axon regeneration of RGCs, and combinatorial expression of *Lhx2* and ciliary neurotrophic factor (CNTF) strongly induced long-distance axon regeneration. Further, *Lhx2* overexpression relieved RGC damage or death in ONC, N-methyl-D-aspartate (NMDA)-induced excitotoxic damage of RGC, and microbead-induced mouse glaucoma models. Finally, mechanistic analysis revealed that *Lhx2* downregulates Semaphorin 3C (*Sema3C*), a critical axon-repulsive molecule. Notably, *Sema3C* overexpression abolished the role of *Lhx2* in promoting axon regeneration, but not survival, of RGCs. Collectively, our results suggested that the protective effect of *Lhx2*-mediated survival of RGCs could promote optic nerve axon regeneration and restore visual function, highlighting its therapeutic potential for glaucoma diseases.

RESULTS

Overexpression of *Lhx2* promotes axon regeneration of RGCs in the ONC model

To investigate the function of *Lhx2* in RGCs, we implemented intravitreal injection for adeno-associated virus 2 (AAV2)-mediated overexpression of *Lhx2* (hereinafter referred to as AAV2-LHX2) into RGCs in 6- to 8-week-old mice. Control mice were injected with AAV2-placental alkaline phosphatase (hereinafter referred

to as AAV2-control).²¹ We found that this injection strategy was effective in transducing more than 85% of RGCs (Figures S1A–S1C). Two weeks after the virus injection, the optic nerve was crushed. To detect optic nerve axon regeneration, the anterograde axonal tracer cholera toxin subunit B was injected into the vitreous cavity (Figure 1A). Compared with the control group, where only a small number of axons were able to cross the crush site, overexpression of *Lhx2* significantly promoted axon regeneration at 2 weeks after ONC (Figures 1B and 1C). Notably, some axon lengths reached 2 mm long after recovery (Figures 1B and 1C). To determine the long-term effect of *Lhx2* overexpression, we then tested the length of the regenerating axons 6 weeks after ONC. We found that the longest axon could regenerate up to 3–4 mm (Figures S1D–S1E). In addition, *Lhx2* overexpression could promote axon growth of RGCs (Tuj1⁺) 3 and 9 days after RGC culture *in vitro* (Figure S2). Therefore, we concluded that *Lhx2* overexpression promoted the axon regeneration of RGCs in a prophylactic setting using the ONC model.

To explore the translational potential of *Lhx2* in clinical applications, we tested whether *Lhx2* could promote axon regeneration of RGCs immediately after the injury where AAV2 virus (AAV2-LHX2 and AAV2-control) was injected intravitreally instantly after ONC (Figure 1D). Compared with the control group, *Lhx2* overexpression markedly increased axon regeneration of injured RGCs, with the longest axons up to 2 mm 2 weeks after ONC (Figures 1E–1F). During CNS injury, a large number of neurons undergo cell death in the early stage, while the surviving neurons enter into a “dormant state,” which can be activated later into the axon regeneration mode by environmental stimuli or axon-regeneration-related gene expression.^{39,40} Therefore, we investigated whether *Lhx2* could promote neuronal regeneration of these surviving RGCs on which we performed intravitreal injection of AAV2-LHX2 and AAV2-control 2 weeks after ONC (Figure S3A). The results demonstrated that overexpression of *Lhx2* promoted axon regeneration of these surviving RGCs (Figures S3B and S3C), indicating that *Lhx2* could promote dormant RGCs into the regenerating state after injury. Taken together, these results demonstrated that overexpression of *Lhx2* promoted axon regeneration of RGCs after axonal injury.

CNTF, a potent neurotrophic factor, has been known to protect RGC survival and induce axon regeneration after optic nerve injury.^{41–44} Importantly, CNTF has been clinically tested in glaucoma, retinitis pigmentosa, and ischemic optic neuropathy.⁴⁵ To evaluate the combinational effects of *Lhx2* and *Cntf* overexpression, we performed AAV2-LHX2 and AAV2-CNTF co-injection to examine whether these two factors could synergistically promote post-injury axon regeneration of RGCs. We found that co-expression of *Lhx2* and *Cntf* dramatically induced axon regeneration of RGCs post-injury, showing twice the regenerating axon numbers of those of *Cntf* individual treatment at a 0.25 or 0.5 mm distance from the injury site, and the function of *Lhx2* alone was similar to the combination of *Lhx2* and *Cntf* in the sites 0.75, 1, and 1.25 mm away from the injury site (Figures 1D and 1F). Of note, 8 weeks after ONC, the longest axon distance that regenerating RGCs of the *Lhx2* and *Cntf* co-expressing group could regenerate to was 3–4 mm (Figures S3D and S3E). Therefore, these results demonstrated the translational potential of *Lhx2* gain of function for enhancing axon regeneration in the CNS.

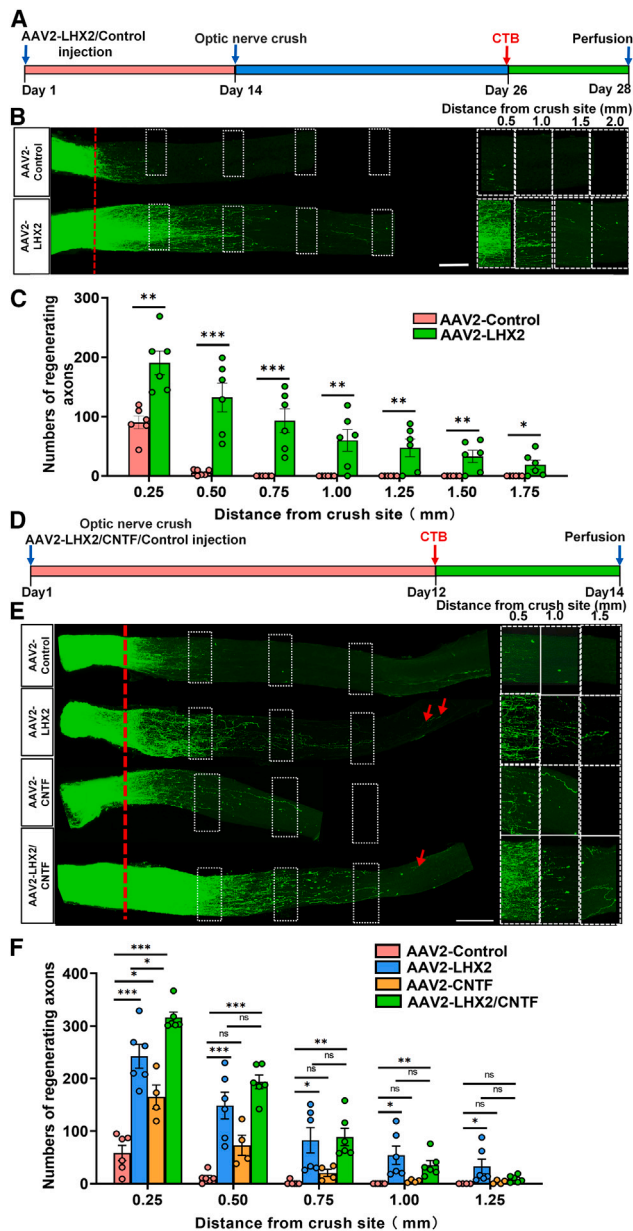


Figure 1. *Lhx2* promotes axon regeneration of RGCs after optic nerve crush

(A) Scheme of the experimental timeline. (B) Axon regeneration was analyzed by cholera toxin subunit B (CTB)-555 tracing. Left, confocal images of optic nerves showing that overexpression of *Lhx2* induced significant axon regeneration 2 weeks after optic nerve crush; red dashed lines represent the crush site. Right, the columns display the magnified axon images of the areas in white dashed rectangles at 0.5, 1.0, 1.75, and 2.0 mm distal to the crush sites. Scale bar, 250 μ m. (C) Quantification of regenerating axons at different distances distal to the nerve crush site (0.25–2.0 mm) (data are presented as mean \pm SEM, one-way ANOVA followed by Tukey's multiple comparisons; * p < 0.05, ** p < 0.01, and *** p < 0.001; AAV2-control, n = 6 mice, AAV2-LHX2, n = 5 mice). (D) Timeline of the experiment. (E) Left, confocal images of optic nerves showing that *Lhx2* and *Cntf* co-expression induced robust axon regeneration 2 weeks after optic nerve crush; red dashed lines represent the crush site, and red arrows indicate the longest

Overexpression of *Lhx2* protects RGC survival in axonal injury and mouse glaucoma models

To determine whether *Lhx2* has a protective effect on neuronal survival, we detected the RGC survival rate using ONC and NMDA-induced excitotoxicity models (Figure 2A). At 14 or 28 days after ONC, the rate of surviving RBPMS⁺ RGCs doubled (~55% or ~38%) in *Lhx2*-treated retinas compared to that in the control group, in which only ~20% or ~15% of RGCs remained alive (Figures 2B–2D).

Glaucoma disease is the second leading cause of blindness in the world.² The primary characteristics of glaucoma are increasing intraocular pressure (IOP)-induced optic nerve impairment and RGC death. Although early detection and appropriate interventions can delay the progression of chronic visual disease, there are still no cures.² NMDA-induced apoptosis of RGCs represents a model of glaucoma in some studies.^{46,47} Using the NMDA-induced excitotoxicity model, we found that *Lhx2* significantly improved the survival of RGCs by more than 2 times (~73% or ~53% at 7 or 14 days after the NMDA injection, respectively) in the treated retinas compared to the control group (~29% or ~12%) (Figures 2E–2G). We also examined axon survival in optic nerve semithin sections collected at 1 mm behind the eyeball and found that *Lhx2* overexpression provided significant protection of RGC axons 7 days after NMDA injection (Figures S4A and S4B). Previous studies have reported that the increase of IOP is a major risk factor for the development and progression of glaucoma, which leads to optic nerve damage and subsequent death of RGCs.^{48,49} We further investigated the translational potential by using another mouse glaucoma model based on the injection of magnetic beads.⁵⁰ We performed intravitreal injections of AAV-LHX2 and AAV-control 2 weeks prior to bead injection (Figures 2H and 2I). Intraocular hypertension was successfully established for 4 weeks after bead injection in both groups (Figure 2J), and the RGC survival rate in the *Lhx2*-treated group was significantly higher than the control using RBPMS labeling (Figures 2K–2L) and optic nerve histological section (Figures S4C and S4D), suggesting that *Lhx2* could maintain RGC survival under high IOP in this glaucoma mouse model. Taken together, these results demonstrated the potential of *Lhx2* overexpression in protecting RGC survival in the models of ONC, NMDA-induced excitotoxicity, and microbead-induced glaucoma.

Lhx2 preserves functional vision in an NMDA-induced excitotoxicity model

Previous research has shown that excitotoxicity is related to multi-neurological diseases, such as ischemic stroke, epilepsy, glaucoma, Alzheimer's disease, and others.^{51–55} Our results

axons of the optic nerve. Right, the columns display the enlarged axon images of the areas in white dashed rectangles at 0.5, 1.0, and 1.5 mm distal to the crush sites. Scale bar, 250 μ m.

(F) Quantification of regenerating axons at different distances distal to the nerve crush site (0.25–1.5 mm) (data are presented as mean \pm SEM, one-way ANOVA followed by Tukey's multiple comparisons test; ** p < 0.01 and *** p < 0.001, ns, not significant; AAV2-control: n = 6 mice, AAV2-LHX2: n = 6 mice, AAV2-CNTF: n = 4 mice, AAV2-LHX2/CNTF: n = 6 mice).

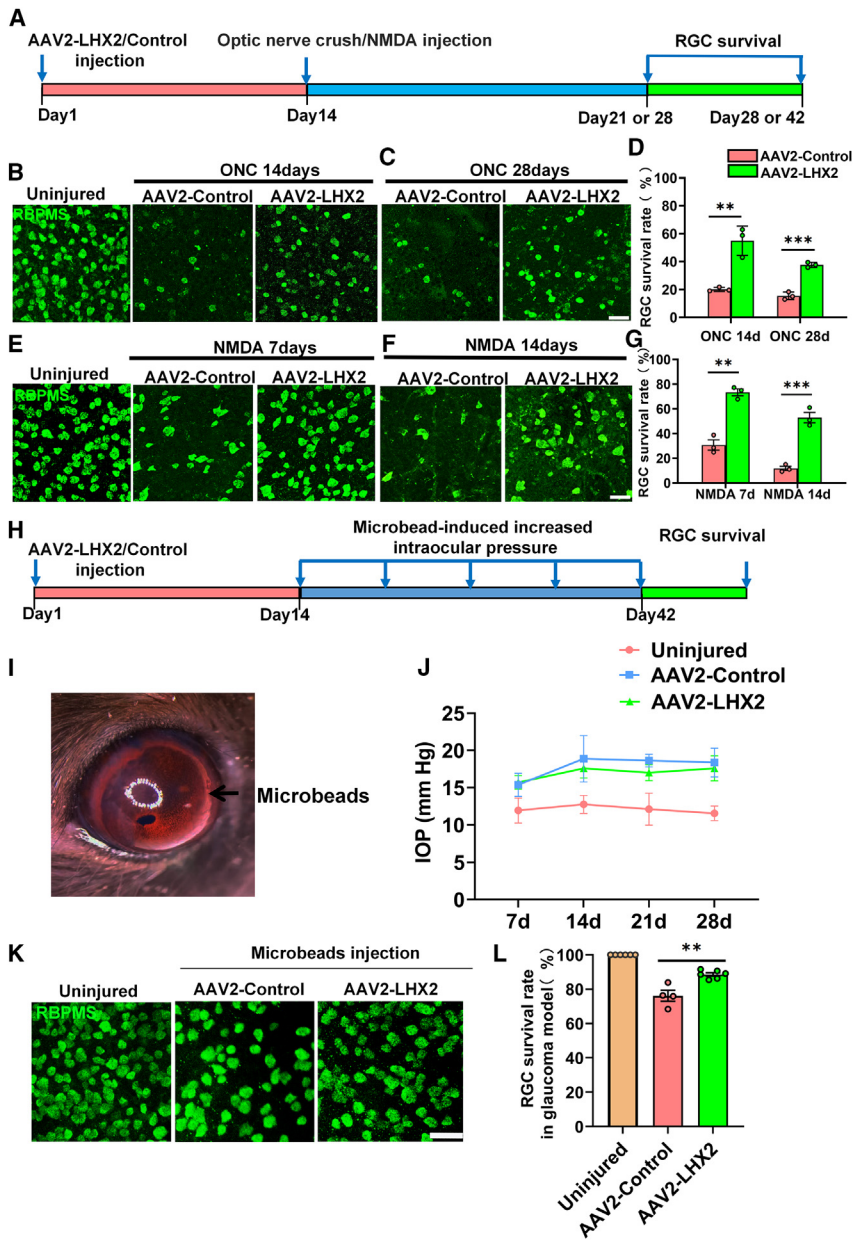


Figure 2. *Lhx2* supports RGC survival in the models of optic nerve crush, NMDA-induced excitotoxicity, and microbead-induced glaucoma

(A) Time course of the experiment. (B and C) Confocal images of retinal whole mounts showing surviving RGCs labeled by RBPMS immunoreactivity (green) 14 (B) and 28 (C) days after optic nerve crush. Scale bar, 50 μ m. (D) Quantification of RGC survival rate after *Lhx2* overexpression 14 and 28 days after optic nerve crush (data are presented as mean \pm SEM, one-way ANOVA followed by Tukey's multiple comparisons; ** $p < 0.01$ and *** $p < 0.001$; $n = 3$ retinas per group; 7–8 fields were analyzed for each retina). (E and F) Confocal images of retinal whole mounts showing surviving RGCs labeled by RBPMS immunoreactivity (green) 7 (E) and 14 (F) days after NMDA injection. Scale bar, 50 μ m. (G) Quantification of RGC survival rate after *Lhx2* overexpression 7 and 14 days after NMDA injection. (data are presented as mean \pm SEM, one-way ANOVA followed by Tukey's multiple comparisons; ** $p < 0.01$ and *** $p < 0.001$; $n = 3$ retinas per group; 7–8 fields were analyzed for each retina). (H) Time course of the experiment. (I) Image of magnetic microbeads distributed along the anterior chamber after injection. (J) Quantification of intraocular pressure (IOP) for the 4 weeks after microbead injection in the AAV2-LHX2 and AAV2-control groups (AAV2-control, $n = 4$ mice; AAV2-LHX2, $n = 6$ mice). (K) Confocal images of retinal whole mounts showing surviving RGCs labeled by RBPMS (green) immunoreactivity of uninjured eyes and AAV2-control- and AAV2-LHX2-treated eyes 4 weeks after induction of elevated IOP. Scale bar, 50 μ m. (L) Quantification of RGC survival rate 4 weeks after induction of elevated IOP in AAV2-control or AAV2-LHX2 group (data are presented as mean \pm SEM; unpaired two-tailed t test; ** $p < 0.01$; uninjured: $n = 6$ mice, AAV2-control: $n = 4$ mice, LHX2: $n = 6$ mice; 7–8 fields were analyzed for each retina).

have indicated that *Lhx2* overexpression could protect RGC and axon survival in the NMDA-induced excitotoxicity model (Figures 2E–2G, S3A, and S3B). Therefore, we hypothesized that *Lhx2* overexpression may restore the function of vision damaged by NMDA-mediated excitotoxicity. To test this idea, we evaluated the electrical signal activity of RGCs in NMDA-injected mice by visual electrophysiology including pattern electroretinogram (PERG) and photopic negative response (PhNR) (Figure 3A).^{56,57} PERG is an electrophysiological ophthalmologic test that provides a non-invasive, objective, quantitative measurement of central retinal function.⁵⁶ We first tested whether *Lhx2* treatment could maintain RGC function by using PERG and found that the peak-to-trough (P50-N95) amplitude ratio of the injured eyes to the normal eyes significantly

increased after *Lhx2* overexpression in RGCs (Figures 3B and 3C). PhNR is a slow negative component of the full-field electroretinogram for RGC activity.⁵⁷ PhNR responses were readily detectable in normal retinas but significantly reduced after NMDA injection, reflecting a severe loss of RGC function after NMDA-induced excitotoxicity. The PhNR response of RGCs was significantly enhanced after AAV2-Lhx2 injection compared to that in the control group (Figures 3D and 3E). Furthermore, to test whether functional vision could be preserved, we performed the visual acuity under different grating intensity stimuli as detected by optokinetic tracking response.⁵⁸ Consistent with the electrophysiological results, we found that post-treatment with *Lhx2* significantly preserved visual acuity in the NMDA-induced excitotoxicity model (Figures 3F and 3G). All together, these results provided *in vivo* evidence supporting the notion that *Lhx2*-mediated RGC protection could preserve functional vision.

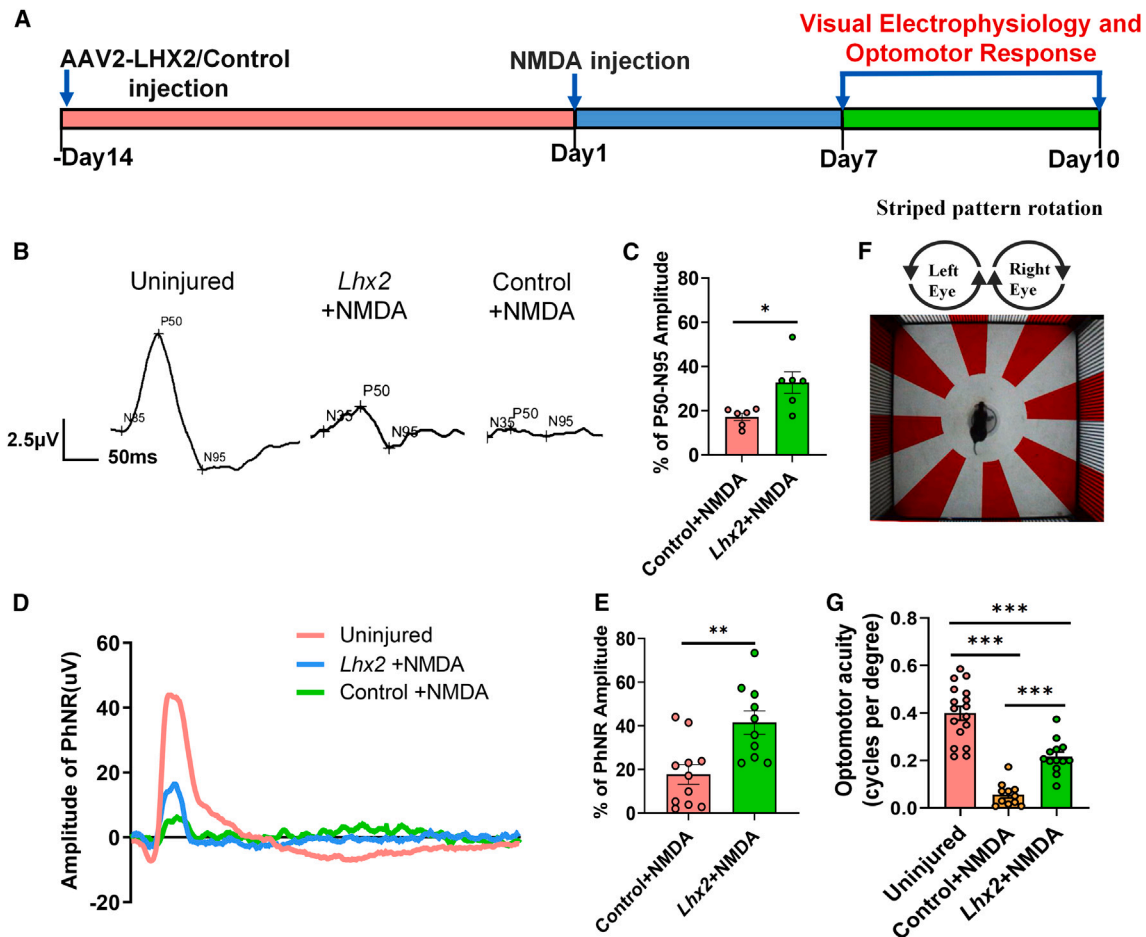


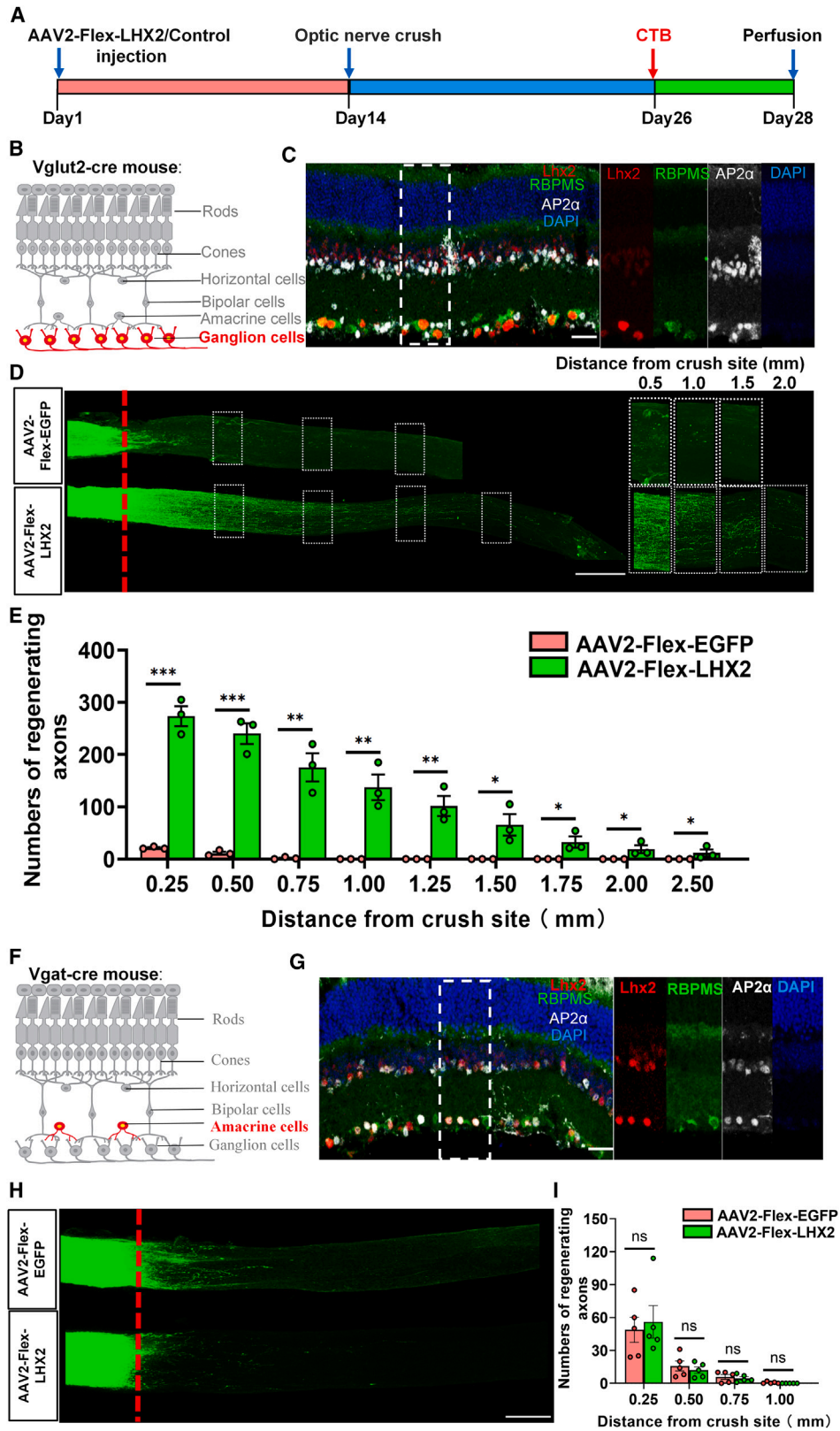
Figure 3. *Lhx2* preserves vision function after NMDA-induced excitotoxicity injury

(A) Time course of the experiment.
 (B) Representative PERG waveforms from uninjured eyes 7 days after NMDA injection in AAV2-control- and AAV2-LHX2-treated eyes.
 (C) Quantification of PERG amplitudes representing the percentage of AAV2-control- or AAV2-LHX2-treated eyes compared to uninjured eyes (data are presented as means \pm SEM; unpaired two-tailed t test; * $p < 0.05$; $n = 6$ in both groups).
 (D) Representative PhNR waveforms of uninjured eyes 7 days after NMDA injection in AAV2-control- and AAV2-LHX2-treated eyes.
 (E) Quantification of PhNR amplitudes representing the percentage of AAV2-control- or AAV2-LHX2-treated eyes compared to uninjured eyes (data are presented as means \pm SEM; unpaired two-tailed t test; ** $p < 0.01$; $n = 11$ mice in per group).
 (F) Image of visual acuity measured by optomotor response.
 (G) Quantification of visual acuity at 7 days after NMDA injection in AAV2-control and AAV2-LHX2 groups (data are presented as means \pm SEM; unpaired two-tailed t test; *** $p < 0.001$; intact: $n = 17$, control+NMDA: $n = 11$, *Lhx2*+NMDA: $n = 13$).

***Lhx2*-mediated axon regenerative and soma survival effects are specific for RGCs**

Lhx2 is highly expressed in RPCs and has a very low expression level in adult RGCs.³⁷ At the adult stage, *Lhx2* is mainly expressed in Müller cells and inhibitory interneurons in retina.^{33,34} The promoter used for AAV constructs is CAG, a non-specific promoter that may produce ectopic expression of transgenes in retinal cells other than RGCs when delivered to wild-type mice. Therefore, we investigated whether *Lhx2*-overexpression-induced axon regeneration and RGC survival was RGC specific. We injected AAV2-LHX2 or control (EGFP) in a double-floxed inverse orientation (AAV2-Flex-LHX2 or AAV2-Flex-EGFP) into two Cre transgenic mouse lines (Figure 4A), Vglut2-

Cre and Vgat-Cre, in which *Lhx2* was selectively expressed in either RGCs (Vglut2-Cre) (Figures 4B and 4C) or inhibitory interneurons (Vgat-Cre), respectively (Figures 4F and 4G). We found that *Lhx2* expression in RGCs alone could promote dramatic axon regeneration (Figures 4D and 4E) but not in inhibitory interneurons (Figures 4H and 4I). Similarly, *Lhx2* expression in RGCs alone could improve cell survival, whereas *Lhx2* expression in inhibitory interneurons had no effect, in the ONC model (Figures S5A and S5B) or the NMDA-induced excitotoxicity model (Figures S5C and S5D). Therefore, these data clearly indicated that the promotional effects of optic nerve axon regeneration and RGC survival induced by *Lhx2* gain of function were a direct result of RGCs.



(legend on next page)

Lhx2 induces global changes of the RGC transcriptome

To gain mechanistic insights into how *Lhx2* promotes axon regeneration of RGCs, we profiled the transcriptomic changes induced by *Lhx2* overexpression through bulk RNA sequencing (RNA-seq). We intravitreally injected AAV2-control or AAV2-LHX2 into mice 2 weeks before ONC. RGCs were labeled 3 days after ONC with antibodies against the RGC-selective marker Thy1, which allows RGC enrichment from dissociated retinal cells by fluorescence-activated cell sorting for downstream RNA-seq analysis (Figures 5A and S6B). We identified 4,947 differentially expressed genes (DEGs) between the control and *Lhx2* overexpression groups at the threshold of an adjusted *p* value < 0.05 and a fold change > 1.5. Of note, we found that 2,228 genes were upregulated and 2,719 genes downregulated (Figures S6A and S6C). Strikingly, some of the upregulated DEGs were known to be involved in the regulation of axon growth or regeneration, such as *Akt1* and *Myc*,^{59–61} cell-cell adhesion molecules (*Itgb1*, *Tgfb2*), serine/threonine protein kinase (*Raf1*,^{62,63} *Map2k2*) (Figure 5B). Interestingly, Gene Ontology pathway analysis showed that the downregulated DEGs were enriched in biological pathways related to the regulation of the extracellular matrix, axonogenesis, negative regulation of nerve system development, and neuron projection guidance processes (Figures 5C and S5D). In particular, one of well-known regeneration-related genes, *Klf4*, was downregulated (Figure 5C), suggesting that *Lhx2* is able to re-activate axon growth programs in injured RGCs. Importantly, among the significantly altered genes, several genes are related to axon guidance, including semaphorin 3C (*Sema3C*),⁶⁴ semaphorin 3E (*Sema3E*),⁶⁵ EPH receptor A4 (*EphA4*),⁶⁶ and lipoprotein-receptor related protein 1 (*LRP1*).⁶⁷ Class III semaphorins (SEMA3s) are one of the major classes of axon-repulsive molecules that contribute to the failure of axon regeneration through the neural scar.⁶⁴ We noted that peripheral myelin protein 22 (*Pmp22*), a major component of myelin involved in axon growth regulation and myelination in the peripheral nervous system, was also downregulated.^{68,69} These gene expressions were further confirmed by real-time PCR: *Sema3C*, *Sema3E*, *Pmp22*, and *Klf4* were indeed downregulated, while *Akt1* and *Myc* were upregulated, after *Lhx2* overexpression (Figure 5D). These results implied that *Lhx2* might act to inhibit functions of important neural development genes during axon regeneration processes.

Next, we examined the downstream target genes in *Lhx2*-regulated cascades. *Lhx2* is an evolutionarily conserved TF binding to the -TAATTA- sequence in the target gene promoters.^{70,71} Therefore, we blasted the sequence of promoter regions (Ensembl genome annotation releases) and found -TAATTA- binding sites in the promoter regions of the *Sema3* family (*Sema3A*, *Sema3C*, *Sema3E*) and *Pmp22*. Then, to test whether *Lhx2* occupies the promoter regions of these genes, we performed chromatin immunoprecipitation-qPCR using specific primers flanking the -TAATTA- sequence in N2a cells. The results demonstrated that *Lhx2* was highly enriched at *Sema3C* region 2 (Figures 5E and 5F) and *Pmp22* region 1 (Figures S7E and S7F), but not at *Sema3A* and *Sema3E* promoter regions (-TAATTA-) (Figures S7A and S7D), suggesting that *Sema3C* and *Pmp22* might be the direct downstream targets of *Lhx2*.

Lhx2 promotes axon regeneration of RGCs through downregulating *Sema3C*

We then tested whether *Sema3C* and *Pmp22* are involved in *Lhx2*-mediated axon regeneration through multiple studies. *Sema3C* belongs to the SEMA3 family of neuronal guidance cues, which play a significant role in axon growth and axon guidance.^{8,64,72} Firstly, we examined the expression pattern of *Sema3C* in RGCs and found that it peaks 3 days after optic nerve injury (Figures 6A and 6B). We also verified that the expression of *Sema3C* protein was significantly downregulated when *Lhx2* was introduced (Figures 6C and 6D) by retinal section immunofluorescence, similar to the RNA-seq results that the transcription of *Sema3C* decreased in treated RGCs. Secondly, AAV2-LHX2 and AAV2-*Sema3C* were simultaneously overexpressed in RGCs (AAV2-control, AAV2-LHX2, and AAV2-LHX2/*Sema3C*). Injection was performed 2 weeks before ONC, while the optic nerve regeneration of RGCs was analyzed 2 weeks after ONC (Figure 6E). The results showed that *Lhx2*-mediated axon regeneration of RGCs was nearly neutralized upon overexpression of *Sema3C*, indicating that *Sema3C* restraint was required for *Lhx2*-mediated axon regeneration of RGCs after ONC (Figures 6F and 6G). Thirdly, AAV2-*Sema3C*-short hairpin RNA was constructed and introduced into RGCs, which found that RGC axon regeneration was observed in the *Sema3C* knockdown group (Figures 6F and 6G). However, we found that overexpression of *Pmp22* could not block *Lhx2*-induced axon regeneration of RGCs (Figures S8A and S8C), suggesting

Figure 4. *Lhx2*-mediated axon regeneration is specific to RGCs

- (A) Timeline of the experiment.
 (B) Schematic of the retinal structure of *Vglut2*-Cre mouse expressing *Lhx2* in RGCs specifically.
 (C) Confocal image showing that *Lhx2* (red) was specifically expressed in RBPMS+ (green+) and AP2 α - (white-) labeled RGCs.
 (D) Axon regeneration was analyzed by CTB-555 tracing. Left, confocal images showing that *Lhx2* expression in RGCs induced axon regeneration 14 days after optic nerve crush in *Vglut2*-cre mouse. Right, the columns display magnified images of the areas in the white dashed rectangles at 0.5, 1.0, 1.75, and 2.0 mm distal to the crush sites. Scale bar, 40 μ m.
 (E) Quantification of regenerating axons at different distances distal to the nerve crush site (0.25–2.5 mm) (data are presented as mean \pm SEM; one-way ANOVA followed by Tukey's multiple comparisons test; **p* < 0.05, ***p* < 0.01, and ****p* < 0.001; AAV2-Flex-EGFP: *n* = 3 mice, AAV2-Flex-LHX2: *n* = 3 mice).
 (F) Schematic of retinal structure showing *Vgat2*-cre mouse expressing *Lhx2* in inhibitory neurons specifically.
 (G) Confocal image of RBPMS- (green-) and AP2 α + (white+) labeled inhibitory neuron (amacrine cells) expressing *Lhx2* (red).
 (H) Axon regeneration was analyzed by CTB-555 tracing. Confocal images showing that *Lhx2* overexpression in inhibitory neuron did not induce axon regeneration 14 days after optic nerve crush in *Vgat2*-cre mouse. Scale bar, 250 μ m.
 (I) Quantification of regenerating axons at different distances distal to the nerve crush site (0.25–1.0 mm) (data are presented as mean \pm SEM; one-way ANOVA followed by Tukey's multiple comparisons test; ns, not significant; AAV2-Flex-EGFP: *n* = 5 mice, AAV2-Flex-LHX2: *n* = 5 mice).

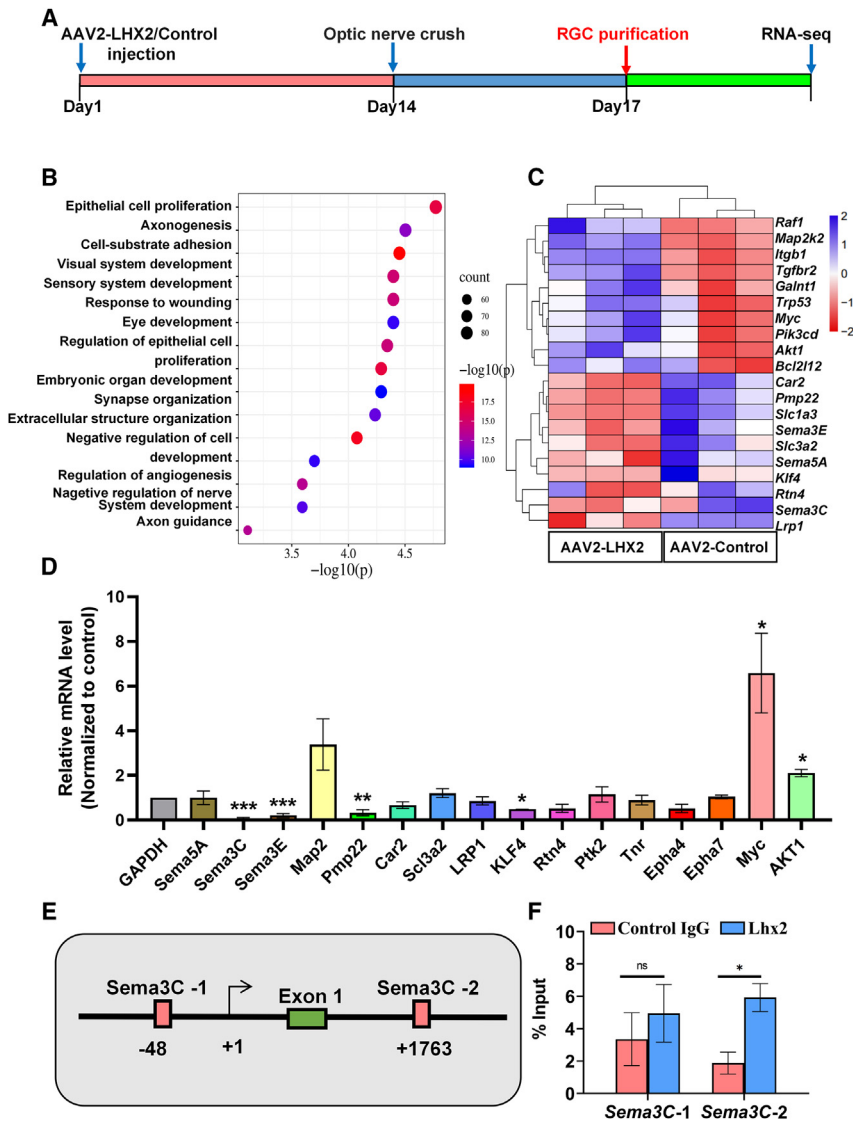


Figure 5. *Lhx2* induces global transcriptome changes in RGCs

(A) Timeline of collecting injured RGCs for bulk RNA-seq after *Lhx2* overexpression.

(B) Gene Ontology analysis of downregulated differentially expressed genes (DEGs) induced by *Lhx2* overexpression.

(C) Heatmaps of up- and downregulated genes enriched for axon guidance, extracellular matrix, and axon regeneration induced by *Lhx2* overexpression.

(D) Real-time PCR analysis of mRNA levels of regeneration-related genes in RGCs following *Lhx2* overexpression; the selection of regeneration-related genes was determined through bulk RNA-seq (data are presented as mean \pm SEM; unpaired two-tailed t test; * p < 0.05, ** p < 0.01, and *** p < 0.001; n = 3).

(E) Scheme image showing *Lhx2*-bound sites (pink boxes indicate 6 bp consensus sequences) at the *Sema3C* gene.

(F) Chromatin immunoprecipitation-qPCR revealed that *Lhx2* was highly enriched in the specific enhancer region (TAATTA) of *Sema3C* in N2a cells (data are presented as mean \pm SEM; unpaired two-tailed t test; * p < 0.05; ns, not significant; control immunoglobulin G [IgG]; n = 3, *Lhx2*: n = 3).

that *Pmp22* was not a functional downstream target of *Lhx2*. In contrast, the RGC survival results showed that RGC survival maintained by overexpression of *Lhx2* was independent of *Sema3C* in ONC (Figures S9A and S9B) and NMDA-induced excitotoxicity (Figures S9C and S9D). Thus, *Sema3C*, as a downstream target of *Lhx2*, was primarily involved in axon regeneration rather than RGC survival.

DISCUSSION

Understanding the mechanism of injured axon regeneration in adult mammals has been a major challenge. Manipulation of intrinsic factors provides new clues for enhancing axon regeneration and functional recovery.^{22–24} For example, many key TFs involved in the transition from RPCs to RGCs during development are highly relevant to the axon growth program.^{21,27–31} By using multiple animal models of optic nerve and retinal injury, our study demonstrated that overexpression of *Lhx2* improved

RGC survival and promoted axon regeneration. The visual signal loss in the NMDA-induced excitotoxicity model was mitigated through *Lhx2* expression. Our results provide a promising molecular target for manipulating regeneration of mature CNS neurons and for functional recovery in neurodegenerative diseases.

As a TF of the LIM family, *Lhx2* is a complex molecule that has different molecular mechanisms through transcription activation or inhibition of different target genes.

A previous study using AAV2 carrying a single-guide RNA (sgRNA) and CRISPR-Cas9 indicates that knockout of *Lhx2* promotes axon regeneration of RGCs.³² However, our results showed that RGC-specific *Lhx2* overexpression promoted axon regeneration. Although these findings seem to be controversial, we reasoned that *Lhx2*-mediated effects might be cell-type specific. *Lhx2* is mainly expressed in Müller cells and inhibitory interneurons in adults^{33,34} and has a very low expression level in adult RGCs, based on recent single-cell RNA-seq data.^{73,74} Consistent with previous studies, intravitreal injection of AAV2 virus transduces most RGCs, some amacrine cells, and other cell types in our experiments.^{23,32} To exclude other cell types, we injected a double-floxed inverse orientation virus (AAV2-Flex-LHX2) into two Cre transgenic mouse lines (Vglut2-Cre and Vgat-Cre) and determined that the promoting effect of RGC survival and axon regeneration of *Lhx2* were RGC intrinsic. In addition, it is possible that downregulation of *Lhx2* in other cell types, such as amacrine cells, may promote axon regeneration of RGCs through cross-talk between these cells and RGCs. A

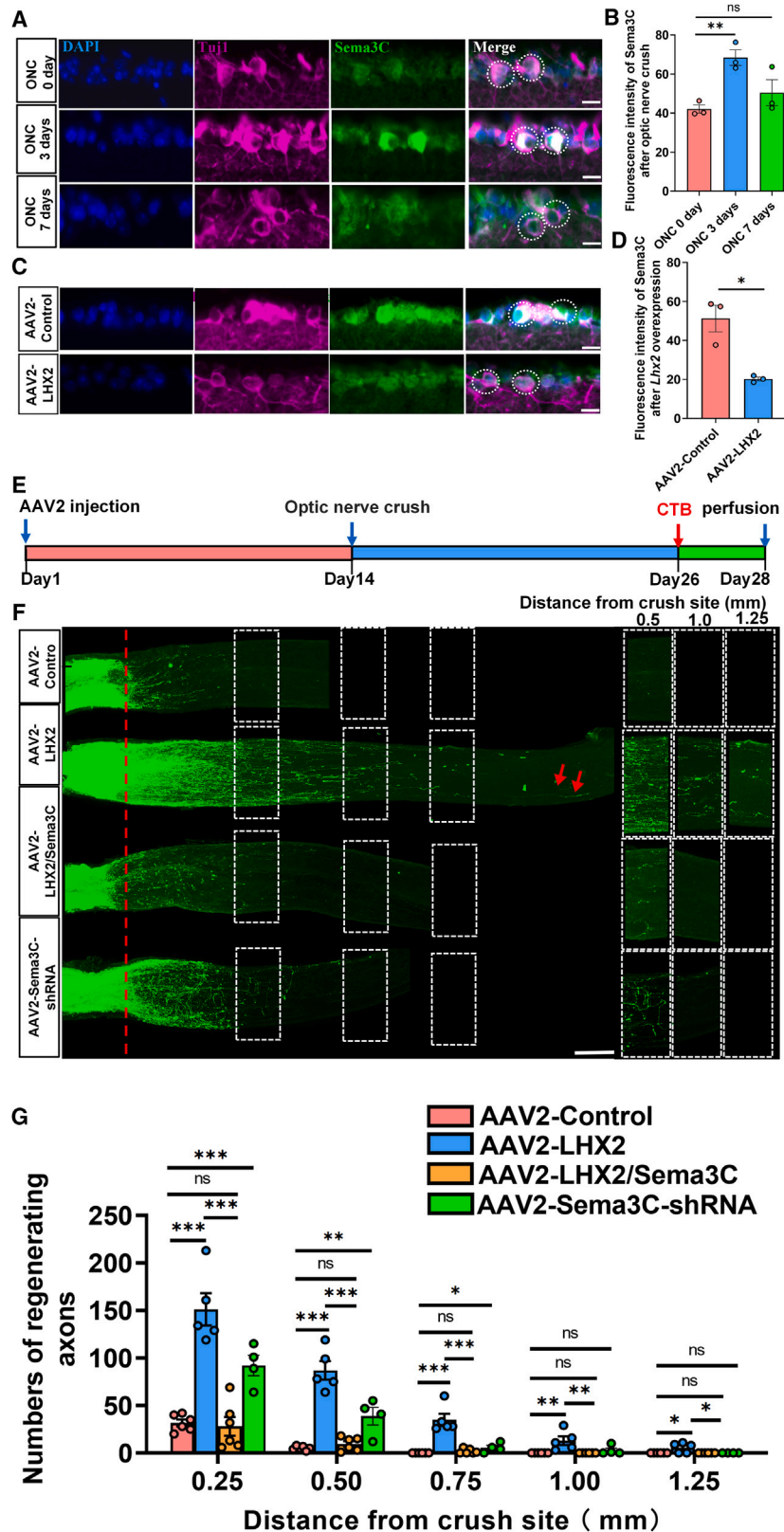


Figure 6. *Lhx2* supports axon regeneration of RGCs by transcriptionally suppressing *Sema3C*

(A) Quantification of immunofluorescence staining results showing Sema3C expression in RGCs after optic nerve crush (0, 3, and 7 days). Co-staining of RGCs with anti-Tuj1 (purple), anti-Sema3C (green), and DAPI (blue). White dashed circle frame indicates Tuj1 and Sema3C co-staining in RGCs. Scale bar, 20 μ m.

(B) Quantification of Sema3C fluorescence intensity in RGCs after optic nerve crush (data are presented as mean \pm SEM; unpaired two-tailed t test; $^{**}p < 0.01$; AAV2-control: $n = 3$ mice, AAV2-LHX2: $n = 3$ mice; 10–15 fields were analyzed for each retina).

(C) Representative images of Sema3C immunofluorescence staining in RGCs with *Lhx2* overexpression. Co-staining of RGCs with anti-Tuj1 (purple), anti-Sema3C (green), and DAPI (blue). White dashed circle frame indicates Tuj1 and Sema3C co-staining in RGCs. Scale bar, 20 μ m.

(D) Quantification of Sema3C fluorescence intensity in RGCs after *Lhx2* overexpression (data are presented as mean \pm SEM; unpaired two-tailed t test; $^{*}p < 0.05$; AAV2-control: $n = 3$ mice, AAV2-LHX2: $n = 3$ mice; 10–15 fields were analyzed for each retina).

(E) Time course of the experiment.

(F) Axon regeneration was analyzed by CTB-555 tracing. Left, confocal images showing that *Lhx2* supported optic nerve regeneration via down-regulating *Sema3C* 2 weeks after optic nerve crush, with red dashed lines representing the crush site and red arrows indicating the longest axons of the optic nerve. Right, the columns display enlarged axon images of the areas in the white dashed rectangles on the left at 0.5, 1.0, and 1.25 mm distal to the crush sites. Scale bar, 250 μ m.

(G) Quantification of regenerating axons at different distances distal to the nerve crush site (0.25–1.25 mm) (data are presented as mean \pm SEM; one-way ANOVA followed by Tukey's multiple comparisons test; $^{*}p < 0.05$ and $^{**}p < 0.01$; ns, not significant; AAV2-control: $n = 6$ mice, AAV2-LHX2: $n = 5$ mice, AAV2-LHX2/Sema3C: $n = 6$ mice, AAV2-Sema3C-short hairpin RNA [shRNA]: $n = 4$ mice).

similar scenario occurs for *Lin28*, which has been demonstrated to promote axon regeneration of RGCs.^{22,75} However, the promoting effect of *Lin28* is not cell intrinsic, as *Lin28* is required in amacrine cells but not RGCs.²³ Overall, our study and the published work indicate that the role of *Lhx2* is very complex, and future explorations of the functions of *Lhx2*, particularly in adult RGCs and other cell types, are needed.

Lhx2 activates or represses the transcription of its target genes through directly binding to their promoters or enhancers.^{33–35,76,77} In the mouse thyrotrope, *Lhx2* stimulates the transcription of the thyroid-stimulating hormone β -subunit.⁷⁸ In humans, *Lhx2* promotes the expression of *Pax6* by binding to the active enhancer regions to regulate the neural differentiation of human embryonic stem cells.⁷⁰ Similarly, *Lhx2* promotes the expression of *Msx1* and *Msx2* as a component of a nuclear factor complex bound to the enhancer region and inhibits the differentiation of skeletal muscle.⁷⁹ On the other hand, *Lhx2* binds to the region near the transcription start site and inhibits the expression of *Robo1* and *Robo2* to control the orientation of thalamic neurons.⁷¹ Likewise, *Lhx2* regulates bone remodeling in mice by inhibiting c-Fos binding in the nuclear factor of activated T cells c1 (*NFATc1*) promoter region, thereby regulating the receptor activator of nuclear factor κ B ligand signaling pathway in osteoclasts.⁸⁰ In this study, we demonstrated that *Lhx2* bound to the conserved binding site TAATTA in the promoter region of *Sema3C* and downregulated the expression of *Sema3C* in RGCs, indicating that *Lhx2* acts as a transcriptional repressor of *Sema3C*. However, it remains unclear whether *Lhx2* alone or in concert with other cofactors to regulate the expression of downstream targets. Future investigations are warranted to define the molecular mechanisms by which *Lhx2* exerts its role as a transcriptional activator or repressor.

Semaphorins were originally identified as a family of genes encoding guidance molecules that play an important role in various neuronal systems as repulsive or attractive axonal guides.^{64,65,81} Particularly, upregulation of *Sema3A*, a secreted protein by neurons and surrounding tissues, can induce axon growth deflection and neuronal cell death, whereas inhibition of *Sema3A* promotes cell migration and axonal growth.⁸² Of note, neutralization of *Sema3A* activity markedly reduces the death of RGCs following optic nerve axotomy in adult rats.⁸³ In addition, the axonal guidance effects of *Sema3A* and *Sema3C* in the mouse hippocampus were observed: *Sema3A* repels neurites from the entorhinal cortex (EC), dentate gyrus (DG), and cornu ammonis (CA) regions CA1 and CA3, but not from the medial septum, whereas *Sema3C* repels neurites from the CA1 and medial septum, but not from the CA3, DG, and EC.⁸ Consistently, following axonal injury, the expression of *Sema3C* is upregulated in injured rodent facial and rubrospinal neurons.⁷² In our study, we found that the expression of *Sema3C* in RGCs was upregulated after ONC and that *Lhx2* overexpression inhibited the expression of *Sema3C* to promote axon regeneration of RGCs. Functionally, overexpression of *Sema3C* blocked axon regeneration of RGCs induced by *Lhx2* overexpression, thus establishing the *Lhx2*-*Sema3C* axis as a negative regulator of axon regeneration in CNS. The number and length of regenerative axons promoted by *Sema3C* knock-down are smaller than those promoted by *Lhx2* overexpression, so there are still some other target genes of *Lhx2* that need further

research to promote RGC axon regeneration. Meanwhile, our data supported that *Lhx2* overexpression promoted RGC survival, which was independent of the overexpression of *Sema3C* in ONC and NMDA-induced excitotoxicity models. Given that transcription programs for regulating axon regeneration and neuronal survival are essentially distinct,³² axon regeneration cannot occur by just sustaining RGC survival.⁸⁴ Neurons overexpressing *bcl-2* are capable of surviving axotomy, and axon regeneration does not occur when faced with an environment where axonal regeneration is inhibited.⁸⁵ *Sox11*, as a developmentally important TFs in adult RGCs, promotes axon regeneration of some RGC types but kills α -RGCs.²¹ We speculate that *Lhx2* regulates RGC somatic survival and axon regeneration via different mechanisms. *Sema3C*, as an axon-guiding molecule, were primarily involved in axon regeneration rather than cell survival.

Successful regenerative strategies are extremely important for the reconstruction of injured CNS axons and future clinical treatment of neurological diseases,^{86,87} especially for long-distance regeneration of injured CNS axons, enhanced neuronal survival, and functional recovery.^{88,89} In the present study, overexpression of *Lhx2* promoted axons to extend continuously at a maximal length of 3–4 mm within 6 weeks after injury. We did observe that *Lhx2* overexpression could still support a limited number of axons arriving via optic chiasma, but the ability of *Lhx2* to promote axon regeneration was gradually diminished beyond 6–8 weeks compared to the time points of 2–6 weeks after injury. We hypothesized that the lack of myelin regeneration and dystrophy would cause the regenerated axons to deteriorate after more than 8 weeks of injury, necessitating combinatorial treatments to enhance axon regeneration. Theoretically, axon regeneration in the CNS is inhibited by both extrinsic and intrinsic factors.^{4,90} So far, multiple signaling molecules have been demonstrated to increase neuronal survival and induce axon regeneration in the CNS, including PTEN, CNTF, SOCS3, *Lin28*, *SOX11*, myosin, and so on.^{19–22,42,91,92} Importantly, CNTF and PTEN are currently the most studied molecules for combination strategies, such as *Cntf/Pten* deletion/*Socs3* deletion and *c-Myc/Cntf/Pten* deletion/*Socs3* deletion.^{20,61} In particular, CNTF, a neurotrophic cytokine, has been approved by the FDA as a neuroprotective treatment for retinal degenerative diseases.⁴⁵ To explore the clinical relevance of *Lhx2*, we combined *Lhx2* and *Cntf* expression and investigated their effects on optic nerve axon regeneration following injury. Our results showed that the post-injury treatment of AAV2-LHX2/CNTF dramatically promoted axon regeneration of RGCs 2 weeks after ONC. Unlike the previous reports using multiple molecules simultaneously,^{20,61,93} our strategy of combining only two molecules (*Lhx2* and *Cntf*) post-injury treatment was able to promote axon regeneration and proximity to the optic chiasm even 6 weeks after ONC, suggesting long-term regenerative capacity. Therefore, future studies are required to explore the effectiveness and safety of the combined use of *Lhx2* and other molecules in synergistically promoting axon regeneration before translating research findings into clinical practice. Furthermore, by using an NMDA-induced excitotoxicity model, we demonstrated that *Lhx2* overexpression not only promoted axon regeneration of RGCs but also preserved functional vision. Importantly, in an IOP-induced mouse glaucoma model, we found that AAV2-mediated *Lhx2* overexpression protected both RGC soma

and axon survival. It would be interesting to investigate whether *Lhx2* has a role in promoting axonal survival after ONC using various methods like real-time imaging and *ex vivo* assays. Collectively, our results reveal an essential role for *Lhx2* in adult RGCs to promote neuronal survival and axon regeneration, highlighting the translational potential of manipulating *Lhx2* for the treatment of nerve injury and neurodegeneration diseases.

Limitations of the study

The present study has revealed that *Lhx2* expression promoted soma survival and axon regeneration of RGCs following axonal damage, but there was no evidence that *Lhx2* plays a part in the process of axonal survival, and it was possible that the phenotype was a combination of axonal survival and regeneration. We used bulk RNA-seq to discover the relevant regeneration pathway of *Lhx2* that regulates RGC survival and regeneration and discovered the key role of *Sema3c* in it. However, due to technical limitations, we were unable to determine which types of RGCs are regulated by *Lhx2* in cell survival and axon regeneration, and single-cell RNA-seq and additional functional experimental verification may be required. In the treatment of glaucoma, the function of *Lhx2* requires other animal models, such as hereditary glaucoma models, to further validate its potential value in clinical applications.

STAR★METHODS

Detailed methods are provided in the online version of this paper and include the following:

- KEY RESOURCES TABLE
- RESOURCE AVAILABILITY
 - Lead contact
 - Materials availability
 - Data and code availability
- EXPERIMENTAL MODEL AND SUBJECT DETAILS
 - Animals
- METHOD DETAILS
 - Constructs
 - Antibodies
 - Intravitreal injection and optic nerve crush
 - NMDA-induced excitotoxicity model
 - Tissue preparation and optic nerve tissue clearing
 - RGCs culture
 - Immunostaining
 - Axon survival
 - Quantification of RGC survival rates
 - RGC purification by fluorescence-activated cell sorting (FACS)
 - Library preparation and RNA sequencing
 - RNA-seq data analysis
 - RT-PCR and Chip-qPCR
 - Electroretinography (ERG)
 - Optomotor response
 - Induction of IOP elevation in mice
 - Analysis of optic nerve regeneration
- QUANTIFICATION AND STATISTICAL ANALYSIS
 - Statistical analysis

SUPPLEMENTAL INFORMATION

Supplemental information can be found online at <https://doi.org/10.1016/j.xcrm.2024.101554>.

ACKNOWLEDGMENTS

This work was financially supported by grants from the National Key Research and Development Program of China Project (2021YFA1101400), the National Science Foundation of China (82271428, 31900690, 82130029, and 91753140), and the Open Project Program of the State Key Laboratory of Stem Cell and Reproductive Biology. The funding bodies played no role in the design of the study, the collection, analysis, and interpretation of data, and/or the writing of the manuscript.

AUTHOR CONTRIBUTIONS

Conceptualization, C.-M.L., N.W., and Z.-Q.T.; supervision, C.-M.L., N.W., and Z.-Q.T.; methodology, C.-P.L. and S.W.; C.-P.L. and S.W. performed the studies; investigation, C.-P.L., S.W., and M.G.; data analysis, C.-P.L., S.W., and M.G.; Y.-Q.S., X.-Q.P., H.-Z.D., and J.Z. shared research materials/resources; Y.-Q.S., X.-Q.P., H.-Z.D., and J.Z. assisted with the study; writing—original draft, C.-P.L., C.-M.L., and S.W.; writing—review & editing, all authors.

DECLARATION OF INTERESTS

The authors declare no competing interests.

Received: June 21, 2023

Revised: March 27, 2024

Accepted: April 12, 2024

Published: May 9, 2024

REFERENCES

1. Mahar, M., and Cavalli, V. (2018). Intrinsic mechanisms of neuronal axon regeneration. *Nat. Rev. Neurosci.* *19*, 323–337. <https://doi.org/10.1038/s41583-018-0001-8>.
2. Tham, Y.C., Li, X., Wong, T.Y., Quigley, H.A., Aung, T., and Cheng, C.Y. (2014). Global prevalence of glaucoma and projections of glaucoma burden through 2040: a systematic review and meta-analysis. *Ophthalmology* *121*, 2081–2090. <https://doi.org/10.1016/j.ophtha.2014.05.013>.
3. Liu, K., Tedeschi, A., Park, K.K., and He, Z. (2011). Neuronal intrinsic mechanisms of axon regeneration. *Annu. Rev. Neurosci.* *34*, 131–152. <https://doi.org/10.1146/annurev-neuro-061010-113723>.
4. Li, H.J., Sun, Z.L., Yang, X.T., Zhu, L., and Feng, D.F. (2017). Exploring Optic Nerve Axon Regeneration. *Curr. Neuropharmacol.* *15*, 861–873. <https://doi.org/10.2174/1570159X14666161227150250>.
5. Curcio, M., and Bradke, F. (2018). Axon Regeneration in the Central Nervous System: Facing the Challenges from the Inside. *Annu. Rev. Cell Dev. Biol.* *34*, 495–521. <https://doi.org/10.1146/annurev-cellbio-100617-062508>.
6. Fawcett, J.W., and Verhaagen, J. (2018). Intrinsic Determinants of Axon Regeneration. *Dev. Neurobiol.* *78*, 890–897. <https://doi.org/10.1002/dneu.22637>.
7. Giger, R.J., Hollis, E.R., and Tuszynski, M.H. (2010). Guidance molecules in axon regeneration. *Cold Spring Harbor Perspect. Biol.* *2*, a001867. <https://doi.org/10.1101/cshperspect.a001867>.
8. Steup, A., Lohrum, M., Hamscho, N., Savaskan, N.E., Ninnemann, O., Nitsch, R., Fujisawa, H., Püschel, A.W., and Skutella, T. (2000). *Sema3C* and *netrin-1* differentially affect axon growth in the hippocampal formation. *Mol. Cell. Neurosci.* *15*, 141–155. <https://doi.org/10.1006/mcne.1999.0818>.
9. Rust, R., Grönnert, L., Weber, R.Z., Mulders, G., and Schwab, M.E. (2019). Refueling the Ischemic CNS: Guidance Molecules for Vascular Repair. *Trends Neurosci.* *42*, 644–656. <https://doi.org/10.1016/j.tins.2019.05.006>.
10. Dickendesh, T.L., Baldwin, K.T., Mironova, Y.A., Koriyama, Y., Raiker, S.J., Askew, K.L., Wood, A., Geoffroy, C.G., Zheng, B., Liepmann, C.D.,

- et al. (2012). NgR1 and NgR3 are receptors for chondroitin sulfate proteoglycans. *Nat. Neurosci.* 15, 703–712. <https://doi.org/10.1038/nn.3070>.
11. Fischer, D., He, Z., and Benowitz, L.I. (2004). Counteracting the Nogo receptor enhances optic nerve regeneration if retinal ganglion cells are in an active growth state. *J. Neurosci.* 24, 1646–1651. <https://doi.org/10.1523/JNEUROSCI.5119-03.2004>.
 12. Geoffroy, C.G., and Zheng, B. (2014). Myelin-associated inhibitors in axonal growth after CNS injury. *Curr. Opin. Neurobiol.* 27, 31–38. <https://doi.org/10.1016/j.conb.2014.02.012>.
 13. Fujita, Y., Endo, S., Takai, T., and Yamashita, T. (2011). Myelin suppresses axon regeneration by PIR-B/SHP-mediated inhibition of Trk activity. *EMBO J.* 30, 1389–1401. <https://doi.org/10.1038/emboj.2011.55>.
 14. Schwab, M.E. (2004). Nogo and axon regeneration. *Curr. Opin. Neurobiol.* 14, 118–124. <https://doi.org/10.1016/j.conb.2004.01.004>.
 15. Conceição, R., Evans, R.S., Pearson, C.S., Hânzi, B., Osborne, A., Deshpande, S.S., Martin, K.R., and Barber, A.C. (2019). Expression of Developmentally Important Axon Guidance Cues in the Adult Optic Chiasm. *Invest. Ophthalmol. Vis. Sci.* 60, 4727–4739. <https://doi.org/10.1167/iov.19-26732>.
 16. Hur, E.M., Yang, I.H., Kim, D.H., Byun, J., Zhou, F.Q., Xu, W.L., Xu, W.L., Nicovich, P.R., Cheong, R., Levchenko, A., and Thakor, N. (2011). Engineering neuronal growth cones to promote axon regeneration over inhibitory molecules Saijilafu. *Proc. Natl. Acad. Sci. USA* 108, 5057–5062. <https://doi.org/10.1073/pnas.1011258108>.
 17. Goulart, C.O., Mendonça, H.R., Oliveira, J.T., Savoldi, L.M., Dos Santos Heringer, L., Dos Santos Rodrigues, A., Paes-de-Carvalho, R., and Martinez, A.M.B. (2018). Repulsive Environment Attenuation during Adult Mouse Optic Nerve Regeneration. *Neural Plast.* 2018, 5851914. <https://doi.org/10.1155/2018/5851914>.
 18. Li, S., He, Q., Wang, H., Tang, X., Ho, K.W., Gao, X., Zhang, Q., Shen, Y., Cheung, A., Wong, F., et al. (2015). Injured adult retinal axons with Pten and Socs3 co-deletion reform active synapses with suprachiasmatic neurons. *Neurobiol. Dis.* 73, 366–376. <https://doi.org/10.1016/j.nbd.2014.09.019>.
 19. Park, K.K., Liu, K., Hu, Y., Smith, P.D., Wang, C., Cai, B., Xu, B., Connolly, L., Kramvis, I., Sahin, M., and He, Z. (2008). Promoting axon regeneration in the adult CNS by modulation of the PTEN/mTOR pathway. *Science* 322, 963–966. <https://doi.org/10.1126/science.1161566>.
 20. Sun, F., Park, K.K., Belin, S., Wang, D., Lu, T., Chen, G., Zhang, K., Yeung, C., Feng, G., Yankner, B.A., and He, Z. (2011). Sustained axon regeneration induced by co-deletion of PTEN and SOCS3. *Nature* 480, 372–375. <https://doi.org/10.1038/nature10594>.
 21. Norsworthy, M.W., Bei, F., Kawaguchi, R., Wang, Q., Tran, N.M., Li, Y., Brommer, B., Zhang, Y., Wang, C., Sanes, J.R., et al. (2017). Sox11 Expression Promotes Regeneration of Some Retinal Ganglion Cell Types but Kills Others. *Neuron* 94, 1112–1120.e4. <https://doi.org/10.1016/j.neuron.2017.05.035>.
 22. Wang, X.W., Li, Q., Liu, C.M., Hall, P.A., Jiang, J.J., Katchis, C.D., Kang, S., Dong, B.C., Li, S., and Zhou, F.Q. (2018). Lin28 Signaling Supports Mammalian PNS and CNS Axon Regeneration. *Cell Rep.* 24, 2540–2552.e6. <https://doi.org/10.1016/j.celrep.2018.07.105>.
 23. Zhang, Y., Williams, P.R., Jacobi, A., Wang, C., Goel, A., Hirano, A.A., Brecha, N.C., Kerschensteiner, D., and He, Z. (2019). Elevating Growth Factor Responsiveness and Axon Regeneration by Modulating Presynaptic Inputs. *Neuron* 103, 39–51.e5. <https://doi.org/10.1016/j.neuron.2019.04.033>.
 24. Bray, E.R., Yungher, B.J., Levay, K., Ribeiro, M., Dvoryanchikov, G., Ayupe, A.C., Thakor, K., Marks, V., Randolph, M., Danzi, M.C., et al. (2019). Thrombospondin-1 Mediates Axon Regeneration in Retinal Ganglion Cells. *Neuron* 103, 642–657.e7. <https://doi.org/10.1016/j.neuron.2019.05.044>.
 25. Zhou, F.Q., and Snider, W.D. (2006). Intracellular control of developmental and regenerative axon growth. *Philos. Trans. R. Soc. Lond. B Biol. Sci.* 361, 1575–1592. <https://doi.org/10.1098/rstb.2006.1882>.
 26. Doron-Mandel, E., Fainzilber, M., and Terenzio, M. (2015). Growth control mechanisms in neuronal regeneration. *FEBS Lett.* 589, 1669–1677. <https://doi.org/10.1016/j.febslet.2015.04.046>.
 27. Lyu, J., and Mu, X. (2021). Genetic control of retinal ganglion cell genesis. *Cell. Mol. Life Sci.* 78, 4417–4433. <https://doi.org/10.1007/s00018-021-03814-w>.
 28. Cepko, C. (2014). Intrinsically different retinal progenitor cells produce specific types of progeny. *Nat. Rev. Neurosci.* 15, 615–627. <https://doi.org/10.1038/nrn3767>.
 29. Livesey, F.J., and Cepko, C.L. (2001). Vertebrate neural cell-fate determination: lessons from the retina. *Nat. Rev. Neurosci.* 2, 109–118.
 30. Qin, S., Zou, Y., and Zhang, C.L. (2013). Cross-talk between KLF4 and STAT3 regulates axon regeneration. *Nat. Commun.* 4, 2633. <https://doi.org/10.1038/ncomms3633>.
 31. Lu, Y., Brommer, B., Tian, X., Krishnan, A., Meer, M., Wang, C., Vera, D.L., Zeng, Q., Yu, D., Bonkowski, M.S., et al. (2020). Reprogramming to recover youthful epigenetic information and restore vision. *Nature* 588, 124–129. <https://doi.org/10.1038/s41586-020-2975-4>.
 32. Tian, F., Cheng, Y., Zhou, S., Wang, Q., Monavarfeshani, A., Gao, K., Jiang, W., Kawaguchi, R., Wang, Q., Tang, M., et al. (2022). Core transcription programs controlling injury-induced neurodegeneration of retinal ganglion cells. *Neuron* 110, 2607–2624.e8. <https://doi.org/10.1016/j.neuron.2022.06.003>.
 33. de Melo, J., Miki, K., Rattner, A., Smallwood, P., Zibetti, C., Hirokawa, K., Monuki, E.S., Campochario, P.A., and Blackshaw, S. (2012). Injury-independent induction of reactive gliosis in retina by loss of function of the LIM homeodomain transcription factor Lhx2. *Proc. Natl. Acad. Sci. USA* 109, 4657–4662. <https://doi.org/10.1073/pnas.1107488109>.
 34. de Melo, J., Zibetti, C., Clark, B.S., Hwang, W., Miranda-Angulo, A.L., Qian, J., and Blackshaw, S. (2016). Lhx2 Is an Essential Factor for Retinal Gliogenesis and Notch Signaling. *J. Neurosci.* 36, 2391–2405. <https://doi.org/10.1523/JNEUROSCI.3145-15.2016>.
 35. Chou, S.J., and Tole, S. (2019). Lhx2, an evolutionarily conserved, multifunctional regulator of forebrain development. *Brain Res.* 1705, 1–14. <https://doi.org/10.1016/j.brainres.2018.02.046>.
 36. Yun, S., Saijoh, Y., Hirokawa, K.E., Kopinke, D., Murtaugh, L.C., Monuki, E.S., and Levine, E.M. (2009). Lhx2 links the intrinsic and extrinsic factors that control optic cup formation. *Development* 136, 3895–3906. <https://doi.org/10.1242/dev.041202>.
 37. Gordon, P.J., Yun, S., Clark, A.M., Monuki, E.S., Murtaugh, L.C., and Levine, E.M. (2013). Lhx2 balances progenitor maintenance with neurogenic output and promotes competence state progression in the developing retina. *J. Neurosci.* 33, 12197–12207. <https://doi.org/10.1523/JNEUROSCI.1494-13.2013>.
 38. de Melo, J., Clark, B.S., Venkataraman, A., Shiau, F., Zibetti, C., and Blackshaw, S. (2018). Ldb1- and Rnf12-dependent regulation of Lhx2 controls the relative balance between neurogenesis and gliogenesis in the retina. *Development* 145, dev159970. <https://doi.org/10.1242/dev.159970>.
 39. Tapia, M.L., and Park, K.K. (2022). Awakening dormant neurons long after spinal cord injury. *PLoS Biol.* 20, e3001830. <https://doi.org/10.1371/journal.pbio.3001830>.
 40. Yungher, B.J., Ribeiro, M., and Park, K.K. (2017). Regenerative Responses and Axon Pathfinding of Retinal Ganglion Cells in Chronically Injured Mice. *Invest. Ophthalmol. Vis. Sci.* 58, 1743–1750. <https://doi.org/10.1167/iov.16-19873>.
 41. Cen, L.P., Liang, J.J., Chen, J.H., Harvey, A.R., Ng, T.K., Zhang, M., Pang, C.P., Cui, Q., and Fan, Y.M. (2017). AAV-mediated transfer of RhoA shRNA and CNTF promotes retinal ganglion cell survival and axon regeneration.

- Neuroscience 343, 472–482. <https://doi.org/10.1016/j.neuroscience.2016.12.027>.
42. Leaver, S.G., Cui, Q., Plant, G.W., Arulpragasam, A., Hisheh, S., Verhaagen, J., and Harvey, A.R. (2006). AAV-mediated expression of CNTF promotes long-term survival and regeneration of adult rat retinal ganglion cells. *Gene Ther.* 13, 1328–1341. <https://doi.org/10.1038/sj.gt.3302791>.
 43. Müller, A., Hauk, T.G., and Fischer, D. (2007). Astrocyte-derived CNTF switches mature RGCs to a regenerative state following inflammatory stimulation. *Brain* 130, 3308–3320. <https://doi.org/10.1093/brain/awm257>.
 44. Pernet, V., Joly, S., Dalkara, D., Jordi, N., Schwarz, O., Christ, F., Schaffer, D.V., Flannery, J.G., and Schwab, M.E. (2013). Long-distance axonal regeneration induced by CNTF gene transfer is impaired by axonal misguidance in the injured adult optic nerve. *Neurobiol. Dis.* 51, 202–213. <https://doi.org/10.1016/j.nbd.2012.11.011>.
 45. Fudalej, E., Justyniarska, M., Kasarekto, K., Dziedziak, J., Szaflik, J.P., and Cudnoch-Jędrzejewska, A. (2021). Neuroprotective Factors of the Retina and Their Role in Promoting Survival of Retinal Ganglion Cells: A Review. *Ophthalmic Res.* 64, 345–355. <https://doi.org/10.1159/000514441>.
 46. RJ, C. (2006). Possible role of excitotoxicity in the pathogenesis of glaucoma. *Clin. Exp. Ophthalmol.* 34, 54–56. <https://doi.org/10.1111/j.1442-9071.2006.1146.x>.
 47. EM, B., X, Z., D, M., Q, C., and D, P.-W. (2009). Single-cell imaging of retinal ganglion cell apoptosis with a cell-penetrating, activatable peptide probe in an in vivo glaucoma model. *Proc. Natl. Acad. Sci. USA* 106, 9391–9396.
 48. Leske, M.C., Heijl, A., Hyman, L., and Bengtsson, B. (1999). Early Manifest Glaucoma Trial: design and baseline data. *Ophthalmology* 106, 2144–2153. [https://doi.org/10.1016/s0161-6420\(99\)90497-9](https://doi.org/10.1016/s0161-6420(99)90497-9).
 49. Quigley, H.A., Addicks, E.M., Green, W.R., and Maumenee, A.E. (1981). Optic nerve damage in human glaucoma. II. The site of injury and susceptibility to damage. *Arch. Ophthalmol.* 99, 635–649.
 50. Ito, Y.A., Belforte, N., Cueva Vargas, J.L., and Di Polo, A. (2016). A Magnetic Microbead Occlusion Model to Induce Ocular Hypertension-Dependent Glaucoma in Mice. *J. Vis. Exp.* e53731. <https://doi.org/10.3791/53731>.
 51. Caudle, W.M., and Zhang, J. (2009). Glutamate, excitotoxicity, and programmed cell death in Parkinson disease. *Exp. Neurol.* 220, 230–233. <https://doi.org/10.1016/j.expneurol.2009.09.027>.
 52. Fricker, M., Tolkovsky, A.M., Borutaite, V., Coleman, M., and Brown, G.C. (2018). Neuronal Cell Death. *Physiol. Rev.* 98, 813–880. <https://doi.org/10.1152/physrev.00011.2017>.
 53. Iovino, L., Tremblay, M.E., and Civiero, L. (2020). Glutamate-induced excitotoxicity in Parkinson's disease: The role of glial cells. *J. Pharmacol. Sci.* 144, 151–164. <https://doi.org/10.1016/j.jphs.2020.07.011>.
 54. Izumi, Y., Shimamoto, K., Benz, A.M., Hammerman, S.B., Olney, J.W., and Zorumski, C.F. (2002). Glutamate transporters and retinal excitotoxicity. *Glia* 39, 58–68. <https://doi.org/10.1002/glia.10082>.
 55. Casson, R.J. (2006). Possible role of excitotoxicity in the pathogenesis of glaucoma. *Clin. Exp. Ophthalmol.* 34, 54–63.
 56. Porciatti, V. (2007). The mouse pattern electroretinogram. *Doc. Ophthalmol.* 115, 145–153. <https://doi.org/10.1007/s10633-007-9059-8>.
 57. Prencipe, M., Perossini, T., Brancoli, G., and Perossini, M. (2020). The photopic negative response (PhNR): measurement approaches and utility in glaucoma. *Int. Ophthalmol.* 40, 3565–3576. <https://doi.org/10.1007/s10792-020-01515-0>.
 58. Tabata, H., Shimizu, N., Wada, Y., Miura, K., and Kawano, K. (2010). Initiation of the optokinetic response (OKR) in mice. *J. Vis.* 10, 13.11–17. <https://doi.org/10.1167/10.1.13>.
 59. Guo, X., Snider, W.D., and Chen, B. (2016). GSK3beta regulates AKT-induced central nervous system axon regeneration via an eIF2Bepsilon-dependent, mTORC1-independent pathway. *Elife* 5, e11903. <https://doi.org/10.7554/eLife.11903>.
 60. Luo, J.M., Cen, L.P., Zhang, X.M., Chiang, S.W.Y., Huang, Y., Lin, D., Fan, Y.M., van Rooijen, N., Lam, D.S.C., Pang, C.P., and Cui, Q. (2007). PI3K/akt, JAK/STAT and MEK/ERK pathway inhibition protects retinal ganglion cells via different mechanisms after optic nerve injury. *Eur. J. Neurosci.* 26, 828–842. <https://doi.org/10.1111/j.1460-9568.2007.05718.x>.
 61. Belin, S., Nawabi, H., Wang, C., Tang, S., Latremoliere, A., Warren, P., Schorle, H., Uncu, C., Woolf, C.J., He, Z., and Steen, J.A. (2015). Injury-induced decline of intrinsic regenerative ability revealed by quantitative proteomics. *Neuron* 86, 1000–1014. <https://doi.org/10.1016/j.neuron.2015.03.060>.
 62. Zhong, J., Li, X., McNamee, C., Chen, A.P., Baccarini, M., and Snider, W.D. (2007). Raf kinase signaling functions in sensory neuron differentiation and axon growth in vivo. *Nat. Neurosci.* 10, 598–607.
 63. Annette, M., Jian, Z., and William, D.; Snider (2002). Raf and Akt Mediate Distinct Aspects of Sensory Axon Growth - ScienceDirect. *Neuron* 35, 65–76.
 64. Mecollari, V., Nieuwenhuis, B., and Verhaagen, J. (2014). A perspective on the role of class III semaphorin signaling in central nervous system trauma. *Front. Cell. Neurosci.* 8, 328. <https://doi.org/10.3389/fncel.2014.00328>.
 65. Steffensky, M., Steinbach, K., Schwarz, U., and Schloschauer, B. (2006). Differential impact of semaphorin 3E and 3A on CNS axons. *Int. J. Dev. Neurosci.* 24, 65–72. <https://doi.org/10.1016/j.ijdevneu.2005.10.007>.
 66. Gatto, G., Morales, D., Kania, A., and Klein, R. (2014). EphA4 receptor shedding regulates spinal motor axon guidance. *Curr. Biol.* 24, 2355–2365. <https://doi.org/10.1016/j.cub.2014.08.028>.
 67. Landowski, L.M., Pavez, M., Brown, L.S., Gasperini, R., Taylor, B.V., West, A.K., and Foa, L. (2016). Low-density Lipoprotein Receptor-related Proteins in a Novel Mechanism of Axon Guidance and Peripheral Nerve Regeneration. *J. Biol. Chem.* 291, 1092–1102. <https://doi.org/10.1074/jbc.M115.668996>.
 68. Cavalcanti, F., Kidd, T., Patitucci, A., Valentino, P., Bono, F., Nisticò, R., and Quattrone, A. (2009). An axon regeneration signature in a Charcot-Marie-Tooth disease type 2 patient. *J. Neurogenet.* 23, 324–328. <https://doi.org/10.1080/01677060802447585>.
 69. Shen, Y., Cheng, Z., Chen, S., Zhang, Y., Chen, Q., and Yi, S. (2022). Dysregulated miR-29a-3p/PMP22 Modulates Schwann Cell Proliferation and Migration During Peripheral Nerve Regeneration. *Mol. Neurobiol.* 59, 1058–1072. <https://doi.org/10.1007/s12035-021-02589-2>.
 70. Hou, P.S., Chuang, C.Y., Kao, C.F., Chou, S.J., Stone, L., Ho, H.N., Chien, C.L., and Kuo, H.C. (2013). LHX2 regulates the neural differentiation of human embryonic stem cells via transcriptional modulation of PAX6 and CER1. *Nucleic Acids Res.* 41, 7753–7770. <https://doi.org/10.1093/nar/gkt567>.
 71. Marcos-Mondéjar, P., Peregrín, S., Li, J.Y., Carlsson, L., Tole, S., and López-Bendito, G. (2012). The Lhx2 transcription factor controls thalamocortical axonal guidance by specific regulation of robo1 and robo2 receptors. *J. Neurosci.* 32, 4372–4385. <https://doi.org/10.1523/JNEUROSCI.5851-11.2012>.
 72. Oschipok, L.W., Teh, J., McPhail, L.T., and Tetzlaff, W. (2008). Expression of Semaphorin3C in axotomized rodent facial and rubrospinal neurons. *Neurosci. Lett.* 434, 113–118. <https://doi.org/10.1016/j.neulet.2008.01.048>.
 73. Pouloupoulos, A., Murphy, A.J., Ozkan, A., Davis, P., Hatch, J., Kirchner, R., and Macklis, J.D. (2019). Subcellular transcriptomes and proteomes of developing axon projections in the cerebral cortex. *Nature* 565, 356–360. <https://doi.org/10.1038/s41586-018-0847-y>.
 74. Rheaume, B.A., Jereen, A., Bolisetty, M., Sajid, M.S., Yang, Y., Renna, K., Sun, L., Robson, P., and Trakhtenberg, E.F. (2018). Single cell transcriptome profiling of retinal ganglion cells identifies cellular subtypes. *Nat. Commun.* 9, 2759. <https://doi.org/10.1038/s41467-018-05134-3>.
 75. Nathan, F.M., Ohtake, Y., Wang, S., Jiang, X., Sami, A., Guo, H., Zhou, F.-Q., and Li, S. (2020). Upregulating Lin28a Promotes Axon Regeneration in

- Adult Mice with Optic Nerve and Spinal Cord Injury. *Mol. Ther.* 28, 1902–1917. <https://doi.org/10.1016/j.ymthe.2020.04.010>.
76. Kinare, V., Iyer, A., Padmanabhan, H., Godbole, G., Khan, T., Khatri, Z., Maheshwari, U., Muralidharan, B., and Tole, S. (2020). An evolutionarily conserved Lhx2-Ldb1 interaction regulates the acquisition of hippocampal cell fate and regional identity. *Development* 147, dev187856. <https://doi.org/10.1242/dev.187856>.
 77. Folgueras, A.R., Guo, X., Pasolli, H.A., Stokes, N., Polak, L., Zheng, D., and Fuchs, E. (2013). Architectural niche organization by LHX2 is linked to hair follicle stem cell function. *Cell Stem Cell* 13, 314–327. <https://doi.org/10.1016/j.stem.2013.06.018>.
 78. Kim, K.K., Song, S.B., Kang, K.I., Rhee, M., and Kim, K.E. (2007). Activation of the thyroid-stimulating hormone beta-subunit gene by LIM homeodomain transcription factor Lhx2. *Endocrinology* 148, 3468–3476. <https://doi.org/10.1210/en.2006-1088>.
 79. Kodaka, Y., Tanaka, K., Kitajima, K., Tanegashima, K., Matsuda, R., and Hara, T. (2015). LIM homeobox transcription factor Lhx2 inhibits skeletal muscle differentiation in part via transcriptional activation of Msx1 and Msx2. *Exp. Cell Res.* 331, 309–319. <https://doi.org/10.1016/j.yexcr.2014.11.009>.
 80. Kim, J.H., Youn, B.U., Kim, K., Moon, J.B., Lee, J., Nam, K.I., Park, Y.W., O'Leary, D.D.M., Kim, K.K., and Kim, N. (2014). Lhx2 regulates bone remodeling in mice by modulating RANKL signaling in osteoclasts. *Cell Death Differ.* 21, 1613–1621. <https://doi.org/10.1038/cdd.2014.71>.
 81. Gaur, P., Bielenberg, D.R., Samuel, S., Bose, D., Zhou, Y., Gray, M.J., Dallas, N.A., Fan, F., Xia, L., Lu, J., and Ellis, L.M. (2009). Role of class 3 semaphorins and their receptors in tumor growth and angiogenesis. *Clin. Cancer Res.* 15, 6763–6770. <https://doi.org/10.1158/1078-0432.CCR-09-1810>.
 82. Nitzan, A., Corredor-Sanchez, M., Galron, R., Nahary, L., Safrin, M., Bruzel, M., Moure, A., Bonet, R., Pérez, Y., Bujons, J., et al. (2021). Inhibition of Sema-3A Promotes Cell Migration, Axonal Growth, and Retinal Ganglion Cell Survival. *Transl. Vis. Sci. Technol.* 10, 16. <https://doi.org/10.1167/tvst.10.10.16>.
 83. Shirvan, A., Kimron, M., Holdengreber, V., Ziv, I., Ben-Shaul, Y., Melamed, S., Melamed, E., Barzilai, A., and Solomon, A.S. (2002). Anti-semaphorin 3A antibodies rescue retinal ganglion cells from cell death following optic nerve axotomy. *J. Biol. Chem.* 277, 49799–49807. <https://doi.org/10.1074/jbc.M204793200>.
 84. Williams, P.R., Benowitz, L.I., Goldberg, J.L., and He, Z. (2020). Axon Regeneration in the Mammalian Optic Nerve. *Annu. Rev. Vis. Sci.* 6, 195–213. <https://doi.org/10.1146/annurev-vision-022720-094953>.
 85. Chierzi, S., Strettoi, E., Cenni, M.C., and Maffei, L. (1999). Optic Nerve Crush Axonal Responses in Wild-Type and bcl-2. *J. Neurosci.* 19, 8367–8376.
 86. Nemeth, C.L., Fine, A.S., and Fatemi, A. (2019). Translational challenges in advancing regenerative therapy for treating neurological disorders using nanotechnology. *Adv. Drug Deliv. Rev.* 148, 60–67. <https://doi.org/10.1016/j.addr.2019.05.003>.
 87. McKerracher, L. (2001). Spinal cord repair: strategies to promote axon regeneration. *Neurobiol. Dis.* 8, 11–18. <https://doi.org/10.1006/nbdi.2000.0359>.
 88. Yang, S.G., Li, C.P., Peng, X.Q., Teng, Z.Q., Liu, C.M., and Zhou, F.Q. (2020). Strategies to Promote Long-Distance Optic Nerve Regeneration. *Front. Cell. Neurosci.* 14, 119. <https://doi.org/10.3389/fncel.2020.00119>.
 89. de Lima, S., Habboub, G., and Benowitz, L.I. (2012). Combinatorial therapy stimulates long-distance regeneration, target reinnervation, and partial recovery of vision after optic nerve injury in mice. *Int. Rev. Neurobiol.* 106, 153–172. <https://doi.org/10.1016/B978-0-12-407178-0.00007-7>.
 90. Mar, F.M., Bonni, A., and Sousa, M.M. (2014). Cell intrinsic control of axon regeneration. *EMBO Rep.* 15, 254–263. <https://doi.org/10.1002/embr.201337723>.
 91. Smith, P.D., Sun, F., Park, K.K., Cai, B., Wang, C., Kuwako, K., Martinez-Carrasco, I., Connolly, L., and He, Z. (2009). SOCS3 deletion promotes optic nerve regeneration in vivo. *Neuron* 64, 617–623. <https://doi.org/10.1016/j.neuron.2009.11.021>.
 92. Wang, X.W., Yang, S.G., Zhang, C., Hu, M.W., Qian, J., Ma, J.J., Zhang, Y., Yang, B.B., Weng, Y.L., Ming, G.L., et al. (2020). Knocking Out Non-muscle Myosin II in Retinal Ganglion Cells Promotes Long-Distance Optic Nerve Regeneration. *Cell Rep.* 31, 107537. <https://doi.org/10.1016/j.celrep.2020.107537>.
 93. Kurimoto, T., Yin, Y., Omura, K., Gilbert, H.Y., Kim, D., Cen, L.P., Moko, L., Kügler, S., and Benowitz, L.I. (2010). Long-distance axon regeneration in the mature optic nerve: contributions of oncomodulin, cAMP, and pten gene deletion. *J. Neurosci.* 30, 15654–15663. <https://doi.org/10.1523/JNEUROSCI.4340-10.2010>.
 94. Guo, X., Zhou, J., Starr, C., Mohns, E.J., Li, Y., Chen, E.P., Yoon, Y., Kellner, C.P., Tanaka, K., Wang, H., et al. (2021). Preservation of vision after CaMKII-mediated protection of retinal ganglion cells. *Cell* 184, 4299–4314.e12. <https://doi.org/10.1016/j.cell.2021.06.031>.
 95. Cheng, Y., Wu, S., Yan, X., Liu, Q., Lin, D., Zhang, J., and Wang, N. (2023). Human Pro370Leu Mutant Myocilin Induces the Phenotype of Open-Angle Glaucoma in Transgenic Mice. *Cell. Mol. Neurobiol.* 43, 2021–2033. <https://doi.org/10.1007/s10571-022-01280-x>.
 96. Fang, F., Zhuang, P., Feng, X., Liu, P., Liu, D., Huang, H., Li, L., Chen, W., Liu, L., Sun, Y., et al. (2022). NMNAT2 is downregulated in glaucomatous RGCs, and RGC-specific gene therapy rescues neurodegeneration and visual function. *Mol. Ther.* 30, 1421–1431. <https://doi.org/10.1016/j.ymthe.2022.01.035>.

STAR★METHODS

KEY RESOURCES TABLE

REAGENT or RESOURCE	SOURCE	IDENTIFIER
Antibodies		
Mouse anti-Tubulin b3 (Tuj1)	Biolegend	Cat# ab801202; RRID: AB_10063408
Rabbit anti-RBPMS	Abcam	Cat# ab194213, RRID:AB_2920590
Guinea pig anti-RBPMS	PhosphoSolutions	Cat# 1832-RBPMS, RRID: AB_2492226
Rabbit anti-Lhx2	Abcam	Cat# ab184337, RRID: AB_2916270
Mouse anti-AP2 α	DSHB	Cat# 3b5, RRID: AB_528084
Rabbit anti-Sema3C	Solaibao	Cat# K010031P
Rabbit anti-Pmp22	Solaibao	Cat# K107046P
Alexa Fluor 488 AffiniPure Donkey Anti-Mouse IgG (H + L)	Thermo Fisher Scientific	Cat# A-21202, RRID: AB_141607
Alexa Fluor 647 AffiniPure Donkey Anti-Mouse IgG (H + L)	Thermo Fisher Scientific	Cat# A-31571, RRID: AB_162542
Alexa Fluor 488 AffiniPure Donkey Anti-abbi IgG (H + L)	Thermo Fisher Scientific	Cat# A-21206, RRID: AB_2535792
Alexa Fluor 647 AffiniPure Donkey Anti-Rabbit IgG (H + L)	Thermo Fisher Scientific	Cat# A-31573, RRID: AB_2536183
Alexa Fluor 488 AffiniPure Goat Anti-Guinea pig IgG (H + L)	Thermo Fisher Scientific	Cat# A-11073, RRID: AB_2534117
CD90.2 (Thy-1.2) Monoclonal Antibody	Thermo Fisher Scientific	Cat# 25-0902-82; RRID: AB_469642
Chemicals, peptides, and recombinant proteins		
CTB, Alexa Fluor 555 Conjugate	Thermo Fisher Scientific	Cat#C34775
N-Methyl-D-aspartic Acid (NMDA)	Millipore Sigma	Cat# 454575
Dynabeads M-450 Epoxy	Thermo Fisher Scientific	Cat# 14011
MEM	Gibco	Cat# 11140050
DMEM/F12 (1:1)	Gibco	Cat# 11320033
Neurobasal	Gibco	Cat# 21103049
Opti-MEM reduced serum medium	Thermo Fisher Scientific	Cat#31985-070
GlutaMAX-I	Gibco	Cat# 35050061
HBSS	Thermo Fisher Scientific	Cat# 14175-095
Penicillin-Streptomycin	Hyclone	Cat#SV30010
B-27 (50X)	Gibco	Cat#12587010
T4 DNA Ligase	NEB	Cat#M0202V
Xbal	NEB	Cat# R0145S
BamHI	NEB	Cat# R0136V
Bsal-HF	NEB	Cat#R3535S
Benzyl benzoate ReagentPlus	Sigma-Aldrich	Cat#B6630
Benzyl alcohol anhydrous	Sigma-Aldrich	Cat#305197
T48402-25G,2,2,2-Tribromoethanol	Sigma-Aldrich	Cat#T48402
Lipofectamine 2000	Life Technologies	Cat# 11668019
Critical commercial assays		
FastPure Gel DNA Extraction Mini Kit	Vazyme	DC301-01
2x Phanta® Max Master Mix	Vazyme	P515-01
Papain Dissociation System	Worthington	LK003150
Deposited data		
RNA-seq: Control versus Lhx2 in RGCs after crush	Genome Sequence Archive	GSA: CRAA009539

(Continued on next page)

Continued

REAGENT or RESOURCE	SOURCE	IDENTIFIER
Experimental models: Cell lines		
AAV-293	Procell	CL-0019
Neuro-2a	This study	N/A
Experimental models: Organisms/strains		
Mouse: Vglut2-ires-Cre	Jackson Labs	JAX:028863
Mouse: Vgat-ires-Cre	Jackson Labs	JAX:016962
Mouse:C57BL/6J	SiPeiFu (Beijing)	B204-02
Oligonucleotides		
For all primers, see Table S1	This study	N/A
Recombinant DNA		
AAV2-CAG-LHX2	This study	N/A
AAV2-CAG-GFP	Addgene	Ca#37825
AAV2-CAG-PLAP	This study	N/A
AAV2-CAG-CNTF	This study	N/A
AAV2-Flex-LHX2	VectorBuilder	N/A
AAV2-Flex-EGFP	VectorBuilder	N/A
AAV2-CAG-Sema3C-shRNA	This study	N/A
AAV2-CAG-Sema3C	This study	N/A
AAV2-CAG-Pmp22	This study	N/A
Software and algorithms		
Prism	GraphPad	RRID: SCR_002798
ImageJ	NIH	RRID: SCR_003070
LAS X	Leica	N/A
ZEN 2009 Light Edition	Zeiss	N/A
Other		
Zeiss LSM880 Fast Ariyscan	Zeiss	N/A
BD FACS Fusion	BD Biosciences	N/A
LEICA DMI8	Leica	N/A

RESOURCE AVAILABILITY

Lead contact

Further information and requests for resources should be directed to and will be fulfilled by the lead contact, Chang-Mei Liu (liuchm@ioz.ac.cn).

Materials availability

This study did not generate new reagents.

Data and code availability

- The raw sequence data reported in this paper have been deposited in the Genome Sequence Archive (Genomics, Proteomics & Bioinformatics 2021) in National Genomics Data Center (Nucleic Acids Res 2022), China National Center for Bioinformation/ Beijing Institute of Genomics, Chinese Academy of Sciences (GSA: CRAA009539) that are publicly accessible at <https://ngdc.cncb.ac.cn/gsa>.
- This paper does not generate new code.
- Any additional information required to reanalyze the data reported in this work paper is available from the [lead contact](#) upon request.

EXPERIMENTAL MODEL AND SUBJECT DETAILS

Animals

All mice were from a C57BL/6J genetic background. The Vglut2-ires-Cre mouse line (028863, Jackson Labs) was a kind gift from Dr. Ruimao Zheng's laboratory at Peking University; Vgat-ires-Cre (016962, Jackson Labs) were obtained from Jackson Laboratories.

Mice were housed in specific pathogen-free (SPF)-like conditions, with a maximum of five mice per cage. All mice were maintained in a room at a constant temperature (23°C) with a regular 12-h light/dark cycle with *ad libitum* access to food and water. All animal procedures were approved by the Animal Committee of the Institute of Zoology, Chinese Academy of Sciences, and were conducted in accordance with the guidelines of national ethical regulations for animal care and use in research (IOZ20180025). All mouse surgeries were performed under anesthesia induced by intraperitoneal injection of Tribromoethanol (avertin) (300 mg/kg) diluted in sterile saline. 4-6-week-old C57BL/6J male and female mice were used for excitotoxicity and optic nerve crush, NMDA-induced excitotoxicity, and microbeads-induced mouse glaucoma experiments.

METHOD DETAILS

Constructs

The mouse *Lhx2* open reading frame (ORF) was PCR-amplified from retinal cDNA using a forward primer (5'-CGGGATC-CATGCTGTTCCACAGTCTGT-3') and a reverse primer (5'-CGGAATTCTTAGAAA AGGTTG GTAAGAGTCGTTT -3'). The *Lhx2* ORF with a 5' BamHI restriction site and a 3' EcoRI restriction site was used to replace the *EGFP* open reading frame in AAV2-CAG-EGFP with standard digestion and ligation to generate AAV2-CAG-LHX2. The AAV2-CAG-EGFP was purchased from Addgene (plasmid #37825). Mouse *Sema3C* and *Pmp22* ORFs were amplified from retinal cDNA with a 5' XbaI restriction site and a 3' EcoRI restriction site and used to replace the *EGFP* open reading frame in AAV2-CAG-EGFP to obtain AAV2-CAG-Sema3C, and AAV2-CAG-Pmp22 respectively. Detailed primer sequences can be found in [Table S1](#). AAV2-Flex-LHX2 and AAV2-Flex-EGFP were purchased from VectorBuilder (Yunnan, China). AAV2-PLAP and AAV2-CNTF were purchased from Vigene Biosciences (Jinan, China). The sequence of this shRNA of *Sema3c* was cloned in the vector pAAV-U6-CMV-mCherry to generate AAV2-Sema3c-shRNA. All AAVs were then packaged into AAVs of serotype 2/2 (titers: $\sim 5 \times 10^{12}$ GC/mL) by the Delivectory Biosciences (Beijing, China).

Antibodies

Primary antibodies: Mouse anti-Tuj1 (1:1,000, BioLegend, 801202), Rabbit anti-Lhx2 (1:500, Abcam, ab184337), Rabbit anti-RBPMS (1:500, Abcam, ab194213), Guinea pig anti-RBPMS (1:200, PhosphoSolutions, 1832-RBPMS), Mouse anti-AP2 α (1:50, DSHB, AB_528084), Rabbit anti-Sema3C (1:200, Solaibao, K010031P), Rabbit anti-Pmp22 (1:200, Solaibao, K107046P). Secondary antibodies were from Life Technologies, raised in either goat or donkey against primary antibody's host species, highly cross adsorbed and conjugated to fluorophores of Alexa Fluor 488, Alexa Fluor 568, or Alex Fluor 647, and used at a 1:500-1000 dilution.

Intravitreal injection and optic nerve crush

Intravitreal injection and optic nerve crush were performed as previously described.²² Briefly, mice were anesthetized, 1–2 μ L of AAV2 virus (5×10^{12} GC/mL) was injected into right vitreous humor of the mouse with glass micropipette connected to Microinjection Syringe Pump. The position and direction of glass micropipette were well controlled to avoid injury to the lens. Two weeks after viral injection, mice were anesthetized, the right optic nerve of the mouse was exposed behind the eyeball and crushed with Dumont #5 fine forceps (Fine Science Tools) for 5 s at approximately 0.5 mm behind the optic disc. To label RGC axons in the optic nerve, 2–3 days before perfusion, 1.0 μ L of CTB conjugated with Alexa Fluor 555 (1 μ g/ μ L, Thermo Fisher Scientific) was injected intravitreally with a pulled glass micropipette. Both retina and the right optic nerve were dissected out and post-fixed in 4% PFA overnight at 4°C when harvested.

NMDA-induced excitotoxicity model

For NMDA injection, two weeks after the virus injection, mice were anesthetized, 1.5 μ L NMDA (20 mM, Sigma-Aldrich) was injected into the vitreous humor with a with glass micropipette. The position and direction of the glass micropipette were well controlled to avoid injury to the lens and bleeding.

Tissue preparation and optic nerve tissue clearing

Two days after intravitreal CTB injection, mice were anesthetized and perfused with 0.1 M PBS followed by 4% paraformaldehyde (PFA). Retina and optic nerve were dissected out and post-fixed with 4% PFA overnight at 4°C. Retinas were dehydrated with 30% sucrose overnight at 4°C, and then snap-frozen in OCT. 20 μ m thick sections were cut for retina, adhered to room temperature charged microscope slides, dried, and frozen until further processing. Optic nerve was washed and dehydrated in the increasing concentrations of tetrahydrofuran (50%, 70%, 80%, 100% and 100%, v/v in distilled water, 20 min each) in glass bottles at room temperature, and the dehydrated optic nerves were cleared with a mix solution of benzyl alcohol (BA)/benzyl benzoate (BB) (BA:BB = 1:2 in volume; Sigma) for 20 min. The clearing procedures were kept away from light to reduce the loss of axon fluorescent signal.

RGCs culture

Although pure adult RGCs do not thrive in culture, they perform well in mixed retinal cultures, allowing researchers to study variables and signaling pathways that stimulate RGC axon regeneration. Retinas were dissected, dissociated with papain containing 0.005% DNase (Worthington dissociation system) at 37°C for 10 min, triturated carefully. Cell suspension was pelleted by centrifugation at

500g for 5 min, and resuspended in Neurobasal medium (2% B27, 1% GlutaMAX). Transfer cells to a 6-well plate (previously covered with PDL glass slides) for culture. Cells are incubated for 3 and 9 days at 37°C and 5% CO₂. Three technical repetitions per treatment group are suggested.

Immunostaining

For immunostaining, RGCs were fixed in 4% paraformaldehyde and washed with PBS and blocked in 5% BSA and 0.3% Triton X-100 in PBS for 1 h at room temperature, and then incubated overnight at 4°C in primary antibodies (anti-Tuj1 and anti-Lhx2) diluted in block solution., after washed for three times with PBS, secondary antibodies were applied for 1–2 h at room temperature in block solution. The sections retinas were washed three times with PBS and blocked in 5% donkey serum and 0.3% Triton X-100 in PBS for 1 h at room temperature, and then incubated overnight at 4°C in primary antibodies (anti-RBPMS and anti-Sema3C) diluted in block solution. After washed for three times with PBS, secondary antibodies were applied for 1–2 h at room temperature in block solution. The whole mount retinas immunostaining was performed by following a similar procedure: washed for three times with PBS, blocking in 5% donkey serum and 0.5% Triton X-100 in PBS for 1–2 h at room temperature, incubation for 2 days at 4°C in primary antibody (anti-RBPMS) diluted in block solution, washed for three times with PBS, and incubation with secondary antibodies for 1–2 h at room temperature in block solution.

Axon survival

For axon survival examination, mice were anesthetized and perfused with 0.1 M PBS, optic nerves were fixed in 2.5% glutaraldehyde and 2% paraformaldehyde in 0.1M sodium cacodylate buffer. Optic nerve regions 1 mm distal to the eyeball were embedded in resin. Generate semithin optic nerve cross sections (1 μm) using a microtome Semithin sections of the optic nerve were stained with toluidine blue and imaged with Zeiss LSM 880 microscope equipped with a 100X lens. Quantify the RGC axons in eight non-overlapping areas of each optic nerve section. Axon survival rates was calculated by measuring the ratio of average axon number in optic semithin with NMDA-injection of high IOP to that in uninjured retina.

Quantification of RGC survival rates

For RGC survival rates quantification, the whole-mount retinas were immunostained with rabbit anti-RBPMS antibody to label the surviving RGCs by following the steps described above (see Immunostaining of whole-mount retinas). 6–8 fields were randomly sampled from the peripheral regions of each retina by a 20x lens with Zeiss LSM 880 microscope. RGC survival rates was calculated by measuring the ratio of average RBPMS positive cell number in retina with optic nerve crush or NMDA-injection to that in uninjured retina. The same approach used to analyze the microbeads-induced mouse model of glaucoma.

RGC purification by fluorescence-activated cell sorting (FACS)

RGC purification was performed as described earlier.^{21,31,94} Retinas were dissected, dissociated with papain containing 0.005% DNase (Worthington dissociation system) at 37°C for 10 min, triturated carefully, and dissociated into a single-cell suspension by repeated pipetting in Neurobasal medium containing 4% BSA. Cell suspension was pelleted by centrifugation at 500g for 5 min, and resuspended in Neurobasal medium containing 4% BSA. Cells were blocked with mouse CD16/CD32 Fc blocker antibody (1:50) (BD Pharmingen, 553141) for 5 min on ice to prevent non-specific binding of immunoglobulin to Fc receptors, and then labeled with Thy1.2-PE antibody (1:100) (Biolegend, 105307) for 30 min on ice. Retinal cells were pelleted by centrifugation at 500g for 5 min. Supernatant was discarded and pelleted cells were washed with HBSS containing 4% BSA, pelleted by centrifugation at 500g for 5 min, and resuspended with HBSS. The 7-Amino-Actinomycin D (7-AAD) is a ready-to-use nucleic acid dye that can easily penetrate the damaged membranes of non-viable cells. Cells suspension was then incubated with DAPI and 7-ADD for 5 min before FACS sorting by BD FACSAria Fusion using a 100-micron nozzle. Thy1.2-positive and 7-ADD-negative cells were identified and sorted into HBSS containing 4% BSA.

Library preparation and RNA sequencing

A total amount of 2 μg RNA per sample was used as input material for the RNA sample preparations. Sequencing libraries were generated using NEBNext Ultra RNA Library Prep Kit for Illumina (#E7530L, NEB, USA) following the manufacturer's recommendations and index codes were added to attribute sequences to each sample. Briefly, mRNA was purified from total RNA using poly-T oligo-attached magnetic beads. Fragmentation was carried out using divalent cations under elevated temperature in NEBNext First Strand Synthesis Reaction Buffer (5X). First strand cDNA was synthesized using random hexamer primer and RNase H. Second strand cDNA synthesis was subsequently performed using buffer, dNTPs, DNA polymerase I and RNase H. The library fragments were purified with QiaQuick PCR kits and elution with EB buffer, then terminal repair, A-tailing and adapter adding were implemented. The aimed products were retrieved and PCR was performed, then the library was completed.

RNA concentration of library was measured using Qubit RNA Assay Kit in Qubit 3.0 to quantify RNA and then diluted to 1 ng/μL. Insert size was assessed using the Agilent Bioanalyzer 2100 system (Agilent Technologies, CA, USA), and insert size was accurately quantified using StepOne Plus real-time PCR System (Library valid concentration >10 nM). The clustering of the index-coded

samples was performed on a cBot cluster generation system using HiSeq PE Cluster Kit v4-cBot-HS (Illumina) according to the manufacturer's instructions. After cluster generation, the libraries were sequenced on an Illumina platform and 150 bp paired-end reads were generated.

RNA-seq data analysis

Raw data was saved in FASTQ format, which included the base sequence and quality metadata. Clean data was obtained by filtering out adaptor-polluted or low-quality reads. Bowtie2 mapped clean data to the reference genome, which was then displayed using IGV. MACS2 discovered peaks associated with the genome's open region. The enrichment analysis of GO terms (<http://geneontology.org/>) or KEGG pathways (<http://www.kegg.jp/>) used a hypergeometric test with a threshold $q < 0.05$ to identify significant enrichments.

RT-PCR and Chip-qPCR

Total RNA was isolated from RGCs purified from FACS, and then reverse transcribed into cDNA with TransScript One-Step gDNA Removal and cDNA Synthesis Kit (TRANS). The cDNA was amplified using quantitative SYBR *Premix Ex Taq* (Tli RNaseH Plus) (Takara). Real-time PCR (RT-PCR) was performed using the two-step method RT-PCR system (Roche). Each sample was performed at least in triplicate. mRNA levels were normalized to values for GAPDH using the $2^{-\Delta\Delta C_T}$ method. Detailed primer sequences are in [Table S1](#).

Chromatin immunoprecipitation (ChIP) assay was performed as described earlier. Briefly, Neuro 2A (N2a), is a mouse neural crest-derived cell line that has been extensively used to study neuronal differentiation, axonal growth and signaling pathways, were cross-linked with 1% PFA for 10 min at room temperature and fixation was terminated at 125 mM glycine. The cells were sonicated in SDS lysis buffer on ice, generating soluble chromatin fragments of 100–400 bp. Chromatin was immunoprecipitated with Rabbit anti-Lhx2 (5 μ g, Abcam) and negative control Rabbit anti-IgG (5 μ g, Abcam) antibodies. After incubation, chromatin was pulled down by the Protein A-bound antibodies and washed in IP dilution buffer, TSE-500 solution (0.1% SDS, 1% Triton X-100, 2 mM EDTA, 20 mM Tris, pH 8.1, 500 mM NaCl), Li/Cl wash solution (100 mM Tris, pH 8.1, 300 mM LiCl, 1% NP-40, 1% deoxycholic acid), and 1 \times Tris-EDTA buffer (TE), two times each at 4°C. Protein-DNA complexes were reverse cross-linked in IP elution buffer (50 mM NaHCO₃ and 1% SDS) and incubated with proteinase K (20 mg/ml) and RNase A at 65°C overnight. DNA was extracted with phenol/chloroform/isoamyl alcohol (25:24:1) isolations, precipitated with ethanol and 10 μ g linear acrylamide, and resuspended in nuclease-free water. The DNA was then analyzed by qPCR using specific primers at *Sema3A*, *Sema3C*, *Sema3D*, *Sema3E*, *Sema3F*, and *Pmp22* genes. The qPCR reaction was performed by Roche 480, and the % input was analyzed using the $2^{-\Delta C_T}$ method. Detailed primer sequences are in [Table S1](#).

Electroretinography (ERG)

PERG was recorded as previously reported.^{56,95,96} In brief, animals were dark adapted for at least 12 h prior to recordings. The mice were anesthetized with an intraperitoneal injection of Tribromoethanol (50 mg/kg) and placed on a thermostatically controlled heating pad on the stage of a Ganzfeld recording system (Roland, USA). A golden circle electrode (3 mm diameter) was placed on each eye. Two stainless steel reference electrodes were placed subcutaneously on the cheek and a ground electrode was placed near the base of the tail. For recording the pattern ERG (PERG), the LED-based stimulators were placed in front of the mouse so that the center of the screen was 27.5 cm from the eye. The pattern remained at a contrast of 100% and consisted of three cycles of black-gray elements, with a spatial frequency of 0.05 c/d. Upon stimulation, recordings of 200 traces were averaged to achieve one readout; each trace was recorded up to 500 ms. The first positive peak in the waveform was designated as P50 and the second negative peak as N95. The amplitude was measured from P50 to N95. The mean of the P50–N95 amplitude in the treated/injured eye was compared to that in the control eye to yield a percentage of amplitude change. PhNR was recorded as previously reported,^{57,95} In brief, a drop of 1% Tropicamide (Alcon Laboratories, Australia) was applied to each eye for pupil dilation. Then the PhNR was recorded at the light intensity of 3 cd s/m² in mice that were light adapted for 10 min on a background light intensity of 30 cd/m² 10 sweeps were measured from each animal and results were averaged. The amplitude was measured from b-wave peak to the PhNR trough (PT). The mean of the PT amplitude in the treated/injured eye was compared to that in the control eye to yield a percentage of amplitude change.

Optomotor response

OKR was recorded as previously reported.^{58,96} In brief, visual function was evaluated through a virtual optomotor tracking system (OptoMotry, Lethbridge, Canada). The mouse was placed on an elevated platform in the middle of the testing chamber, which was composed of four computer monitors showing a virtual spatial frequency grating that rotated laterally, and mouse was monitored by a camera set in the ceiling of the chamber. The animals were placed on a platform to adapt for about 5 min. The grating speed was adjusted to 12°/s during the experiment, and the grating spatial frequency ranged from 0.2 to 0.6 cycles/degree (c/d) in a staircase manner. The experimenter selected “Yes” or “No” to indicate whether the animal tracks or does not track the stimulus. The duration of each experiment was 5–10 min, and the interval time for each animal between two adjacent experiments was at least 10 min. Visual function was evaluated by comparing the minimum spatial frequency that could elicit Optomotor Response between different groups.

Induction of IOP elevation in mice

Induction of IOP was recorded as previously reported.^{50,94} In brief, mice were anesthetized. A drop of 1% Tropicamide (Alcon Laboratories, Australia) was applied to each eye for pupil dilation. Elevation of IOP was induced unilaterally by injection of polystyrene microbeads (dynabeads, M-450, Invitrogen) to the anterior chamber of the right eye of each animal under a surgical microscope. Briefly, microbeads were reformulated at a concentration of 1.5×10^6 beads/ μl in PBS. The right cornea was gently punctured near the center using a 34G needle. A small volume (1.5–2 μL) of microbeads was injected through this preformed hole into the anterior chamber via the micropipette. The magnet was used to attract the beads to the iridocorneal angle to ensure that the beads form an evenly distributed ring around the circumference of the anterior chamber. Mice were placed on a heating pad for recovery after the injection.

Analysis of optic nerve regeneration

For tissue-cleared whole-mount optic nerves, Z-stacked (step size: 2 μm) and tiled fluorescent images were obtained with a Zeiss LSM 880 confocal microscope using a 20 \times objective. To accurately quantify the number of optic nerve axon regeneration, every 5 consecutive sections were projected maximum intensity to generate a series of Z-projection images of 10 μm optical section. In each Z-projected image, the number of CTB-labeled fibers was counted at 250 μm intervals from the optic nerve crush site and summed over all Z-projection images.

QUANTIFICATION AND STATISTICAL ANALYSIS

Statistical analysis

GraphPad Prism software was used for statistical analysis. Data in graphs are shown as means \pm SEM. For comparisons between two groups, two-tailed unpaired t test was used. For comparisons among three or more groups, one-way ANOVA followed by Tukey's multiple comparisons was used to determine the statistical significance. Differences between groups with $p < 0.05$ were considered significant (* $p < 0.05$, ** $p < 0.05$, *** $p < 0.01$).